Title
Liver Cancer Initiation Requires p53 Inhibition by CD44-Enhanced Growth Factor Signaling

Journal
Cancer Cell, 33(6)

ISSN
1535-6108

Authors
Dhar, Debanjan
Antonucci, Laura
Nakagawa, Hayato
et al.

Publication Date
2018-06-01

DOI
10.1016/j.ccell.2018.05.003

Peer reviewed

Article

Cancer Cell

Liver Cancer Initiation Requires p53 Inhibition by CD44-Enhanced Growth Factor Signaling

Graphical Abstract

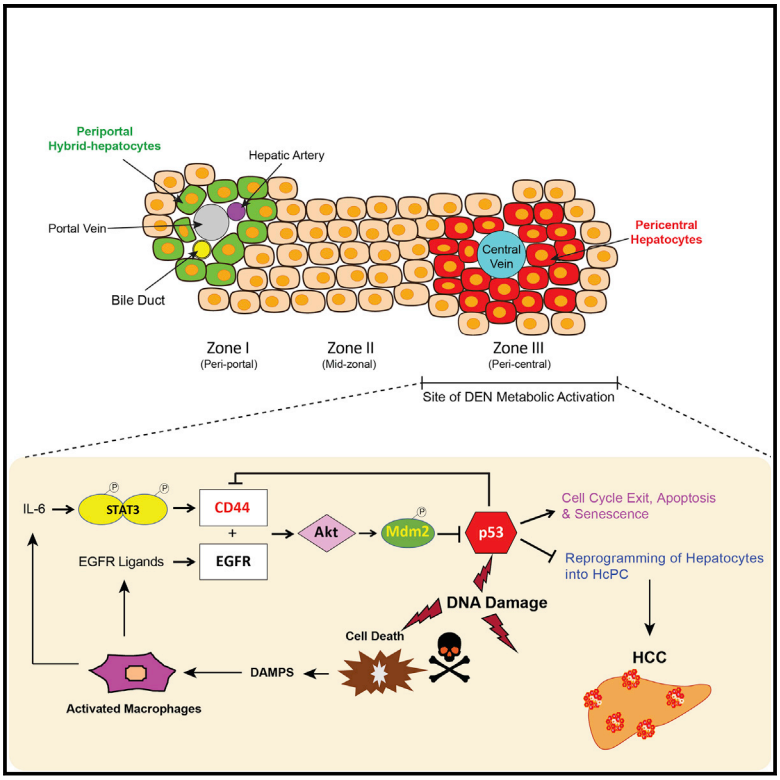

Highlights

- CD44 promotes HCC initiation by protecting DNA-damaged hepatocytes
- MDM2 nuclear translocation is facilitated by CD44-coupled EGFR-AKT signaling axis
- CD44 terminates DNA damage-induced p53 response, cell-cycle exit, and apoptosis
- STAT3 regulates *Cd44* expression in hepatocytes

Authors

Debanjan Dhar, Laura Antonucci, Hayato Nakagawa, ..., Maria Sibilia, Jessica Zucman-Rossi, Michael Karin

Correspondence

karinoffice@ucsd.edu

In Brief

Dhar et al. show that CD44 expression induced in carcinogen-exposed hepatocytes potentiates AKT signaling to activate Mdm2, which terminates the p53 genomic surveillance response. This allows DNA-damaged hepatocytes to respond to proliferative signals, leading their daughter cells to become HCC progenitors.

Dhar et al., 2018, Cancer Cell *33*, 1061–1077
June 11, 2018
https://doi.org/10.1016/j.ccell.2018.05.003

CellPress

Cancer Cell
Article

Liver Cancer Initiation Requires p53 Inhibition by CD44-Enhanced Growth Factor Signaling

Debanjan Dhar,[1] Laura Antonucci,[1] Hayato Nakagawa,[1,5] Ju Youn Kim,[1] Elisabeth Glitzner,[6] Stefano Caruso,[7] Shabnam Shalapour,[1] Ling Yang,[3,8] Mark A. Valasek,[2] Sooyeon Lee,[10] Kerstin Minnich,[11] Ekihiro Seki,[3,9] Jan Tuckermann,[10,11] Maria Sibilia,[6] Jessica Zucman-Rossi,[7] and Michael Karin[1,2,4,12,*]

[1]Laboratory of Gene Regulation and Signal Transduction, Department of Pharmacology, University of California San Diego, School of Medicine, 9500 Gilman Drive, San Diego, CA 92093, USA
[2]Department of Pathology, University of California San Diego, School of Medicine, 9500 Gilman Drive, San Diego, CA 92093, USA
[3]Department of Medicine, University of California San Diego, School of Medicine, 9500 Gilman Drive, San Diego, CA 92093, USA
[4]Moores Cancer Center, University of California San Diego, School of Medicine, 9500 Gilman Drive, La Jolla, CA 92093-0723, USA
[5]Department of Gastroenterology, University of Tokyo, 7-3-1 Hongo, Bunkyo-ku, Tokyo 113-8655, Japan
[6]Institute of Cancer Research, Department of Medicine I, Comprehensive Cancer Center, Medical University of Vienna, Borschkegasse 8a, 1090 Vienna, Austria
[7]Inserm UMR-1162, Génomique Fonctionnelle des Tumeurs Solides, Université Paris Descartes, Université Paris Diderot, Université Paris 13, Labex Immuno-Oncology, 75010 Paris, France
[8]Division of Gastroenterology, Union Hospital, Tongji Medical College, Huazhong University of Science and Technology, Wuhan 430022, China
[9]Department of Medicine, Cedars-Sinai, 8700 Beverly Boulevard, Davis Building, Los Angeles, CA 90048, USA
[10]Institute for Comparative Molecular Endocrinology (CME), University of Ulm, Helmholtzstrasse 8/1, 89081 Ulm, Germany
[11]Leibniz Institute of Age Research-Fritz Lipmann Institute, Beutenbergstrasse 11, 07745 Jena, Germany
[12]Lead Contact
*Correspondence: karinoffice@ucsd.edu
https://doi.org/10.1016/j.ccell.2018.05.003

SUMMARY

How fully differentiated cells that experience carcinogenic insults become proliferative cancer progenitors that acquire multiple initiating mutations is not clear. This question is of particular relevance to hepatocellular carcinoma (HCC), which arises from differentiated hepatocytes. Here we show that one solution to this problem is provided by CD44, a hyaluronic acid receptor whose expression is rapidly induced in carcinogen-exposed hepatocytes in a STAT3-dependent manner. Once expressed, CD44 potentiates AKT activation to induce the phosphorylation and nuclear translocation of Mdm2, which terminates the p53 genomic surveillance response. This allows DNA-damaged hepatocytes to escape p53-induced death and senescence and respond to proliferative signals that promote fixation of mutations and their transmission to daughter cells that go on to become HCC progenitors.

INTRODUCTION

Tumor initiation in response to carcinogenic insults entails induction of oncogenic mutations (Hoeijmakers, 2009; Weinberg, 2013), but exactly how such mutations are acquired by terminally differentiated epithelial cells that rarely divide and give rise to cancer is unknown. A proper answer to this question is essential for understanding the initiation of pancreatic adenocarcinoma (PDAC) and hepatocellular carcinoma (HCC), both of which originate from fully differentiated and rarely dividing epithelial cells, acinar cells (Kopp et al., 2012), and pericentral hepatocytes (Font-Burgada et al., 2015), respectively. Nevertheless, both PDAC and HCC are highly aggressive and difficult-to-treat cancers. Of the two, HCC is a much more common cancer whose development is tightly linked to chronic liver damage and inflammation (El-Serag and Rudolph, 2007).

Significance

Our results explain how fully differentiated epithelial cells, hepatocytes in this case, that experience genotoxic/carcinogenic stress are able to escape the potent p53-dependent genome surveillance checkpoint, survive, divide, and continue to accumulate numerous initiating mutations. Interference with the escape mechanism, which depends on CD44 expression and MDM2 induction, may provide approaches to tumor prevention in tissues, such as liver, that are subject to chronic genotoxic stress.

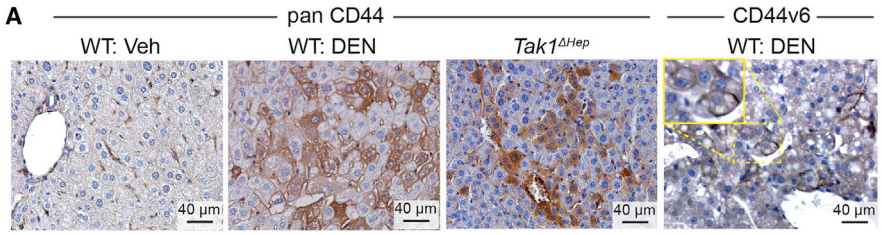

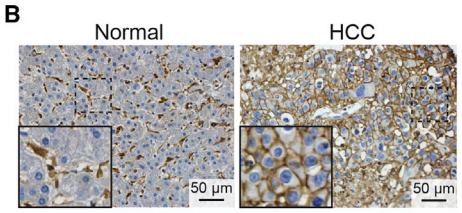

CD44 Staining (Hepatocytes)	Number of HCC Samples	Percentage
Negative	32	53.3%
Positive	28	46.7%

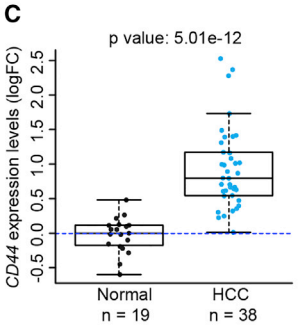

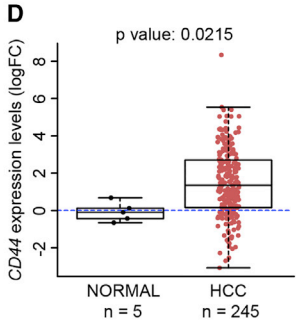

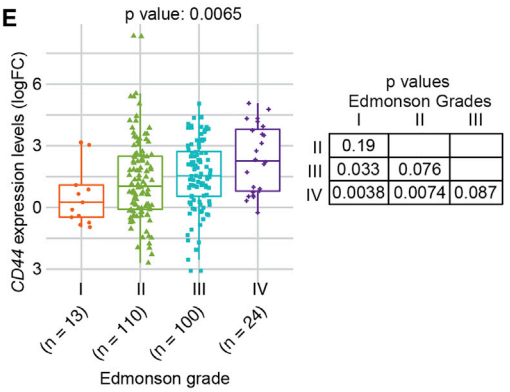

p values Edmonson Grades

	I	II	III
II	0.19		
III	0.033	0.076	
IV	0.0038	0.0074	0.087

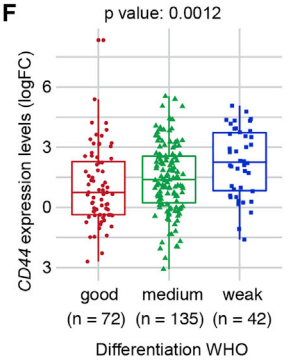

p values Differentiation

	Good	Medium
Medium	0.051	
Weak	0.0005	0.011

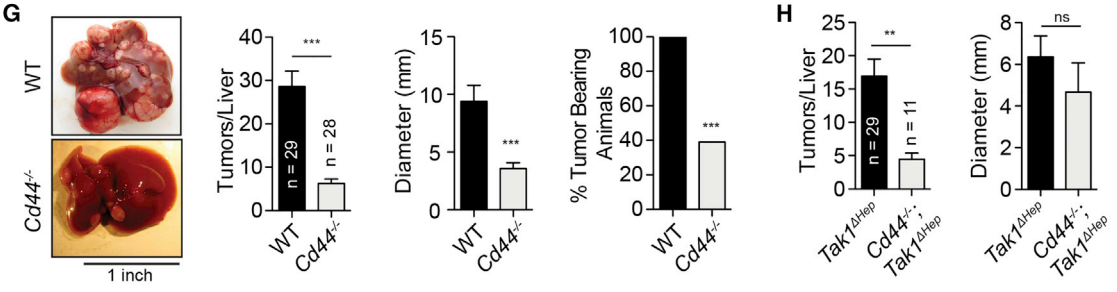

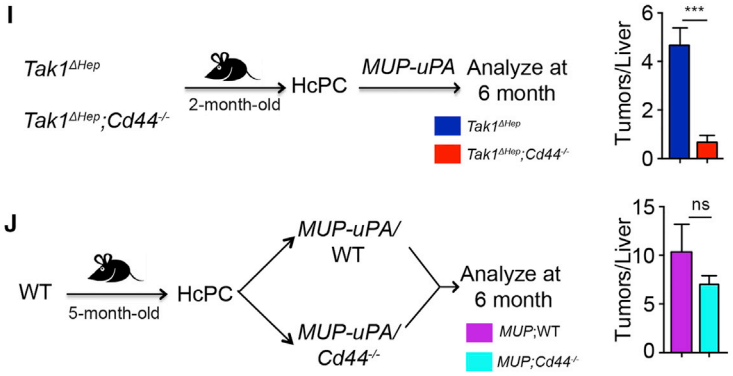

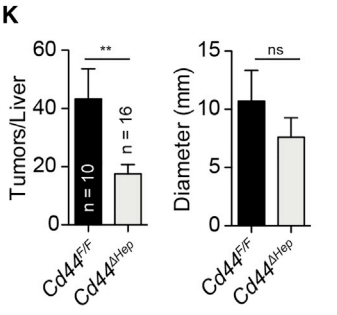

(legend on next page)

The hepatic procarcinogen diethylnitrosamine (DEN) is preferentially metabolized and activated by Cyp2E1-expressing pericentral cells (Kang et al., 2007) to induce HCC that originates from differentiated zone 3 hepatocytes (Font-Burgada et al., 2015). Early in tumor development, differentiated hepatocytes are converted into HCC progenitor cells (HcPCs), which despite their pericentral origin display a transcriptomic signature similar to bipotential hepatobiliary cells (also known as oval cells) that reside periportally (He et al., 2013). Tumors that develop in non-alcoholic steatohepatitis (NASH)-driven HCC models also arise from differentiated pericentral hepatocytes (Font-Burgada et al., 2015), which exhibit higher levels of *de novo* lipogenesis than periportal hepatocytes (Hijmans et al., 2014). Although the cellular origin of HCC has been extensively studied, the mechanisms that convert differentiated hepatocytes to HcPCs are poorly understood. Using mouse models in which HCC is induced by DEN administration or consumption of a high-fat diet (HFD), we found that the key to HCC initiation is hepatocyte proliferation elicited by mitogens produced by liver macrophages that were exposed to damage associated molecular patterns (DAMPs), released by damaged hepatocytes (He et al., 2010; Lanaya et al., 2014; Maeda et al., 2005; Naugler et al., 2007; Park et al., 2010; Sakurai et al., 2008). This proliferative response, known as compensatory proliferation, is needed for maintenance of liver mass and damage repair but does not lead to more than a few rounds of cell division (Font-Burgada et al., 2015). Yet, several months after the initial genotoxic challenge, the liver contains HcPCs that undergo multiple divisions to give rise to fully malignant HCC (He et al., 2013). Importantly, carcinogen challenge and DNA damage also result in induction of the tumor suppressor protein p53, whose activation triggers apoptotic death or cell-cycle withdrawal of DNA-damaged cells (Vousden and Lu, 2002).

CD44 is a receptor for hyaluronic acid, but also binds osteopontin, collagen, and fibronectin (Ponta et al., 2003), which is upregulated in many different types of cancer-initiating cells (CICs) or cancer stem cells (CSCs), as well as rapidly proliferating cells (Zoller, 2011). CD44 also serves as a coreceptor for certain growth factor receptors, including epidermal growth factor receptor (EGFR) and c-Met (Ponta et al., 2003), and participates in nuclear factor (NF)-κB and STAT3 activation (Fitzgerald et al., 2000; Lee et al., 2009). There are several CD44 isoforms encoded by alternatively spliced mRNA (Ponta et al., 2003), the standard isoform (CD44s) stimulates epithelial-to-mesenchymal transition during breast cancer progression (Brown et al., 2011), whereas CD44v6 potentiates c-Met signaling (Orian-Rousseau et al., 2002). Although CD44 was suggested to participate in tissue development and homeostasis and in numerous biological processes, including angiogenesis, hematopoiesis, tissue remodeling, and wound healing (Ponta et al., 2003), CD44-null mice are largely aphenotypic and do not reveal any obvious role of CD44 in normal mouse physiology, other than lymphocyte homing (Protin et al., 1999). Despite its obscure function, CD44 has gained prominence as a CSC marker in various malignancies, including HCC, where it was used for CSC identification together with CD90, CD133, CD24, and EpCAM (Yamashita and Wang, 2013). In addition to serving as a marker, CD44 may be involved in tumor initiation, and was suggested to be a target for the tumor-suppressive activity of p53 (Godar et al., 2008). Given the important role of p53 in genome surveillance and elimination of genotoxically stressed cells, and expression of CD44 in HcPCs but not in normal hepatocytes (He et al., 2013), we postulated that CD44 may play a key role in HCC initiation and asked how terminally differentiated hepatocytes that are subjected to genotoxic challenge give rise to proliferative HcPCs.

RESULTS

CD44 Is Upregulated in Mouse and Human HCC and Is Needed for Tumorigenesis

Under normal conditions, CD44 expression in liver is confined to cells of myeloid origin, such as Kupffer cells and lymphocytes (Flanagan et al., 1989). Neither mouse nor human hepatocytes, which comprise 70% of the liver parenchyma, express CD44 (Figures 1A and 1B); however, during malignant transformation, CD44 is upregulated in HcPCs, which are derived from the initiated hepatocytes (He et al., 2013), and becomes an important CSC marker. To evaluate the role of CD44 in HCC development we used two different mouse HCC models with distinct etiology: (1) DEN-induced HCC, where a single injection of DEN into 15-day-old mice leads to HCC development; and (2) *Tak1*$^{\Delta Hep}$ mice, in which hepatocyte-specific TAK1 ablation leads to spontaneous HCC as a result of progressive liver damage, inflammation, and fibrosis due to reduced AMPK activity, increased mTORC1 activity, and defective initiation of autophagy (Inokuchi-Shimizu et al., 2014). CD44 is upregulated in premalignant

Figure 1. CD44 Is Upregulated in HCC and Is Needed for Its Development

(A) Pan CD44 and CD44v6 IHC of vehicle (Veh) or DEN-challenged 5-month-old WT and 9-month-old *Tak1*$^{\Delta Hep}$ livers.

(B) CD44 IHC of human normal liver and HCC.

(C and D) *CD44* mRNA expression in human normal liver and HCC specimens analyzed using Affymetrix Genome U133A 2.0 array (C) or qRT-PCR (D).

(E and F) Edmonson tumor grading (E) and tumor differentiation (F) were categorized based on *CD44* expression using patient samples shown in (D). For (C–F), the results are expressed as Tukey's boxplots where box indicates the first and third quartiles, bar indicates median, whiskers indicate 1.5 interquartile range (IQR) and data beyond the end of the whiskers represent outliers. Mann-Whitney test was used to test the difference between two groups and Kruskal Wallis test for more than two groups.

(G) Gross morphology of 9-month-old DEN-challenged WT and *Cd44*$^{-/-}$ livers. Tumor multiplicity, tumor size, and tumor incidence were determined.

(H) Tumor multiplicity and tumor size in 9-month-old *Tak1*$^{\Delta Hep}$ and *Cd44*$^{-/-}$;*Tak1*$^{\Delta Hep}$ livers.

(I) 10^4 HcPCs from 2-month-old *Tak1*$^{\Delta Hep}$ and *Cd44*$^{-/-}$;*Tak1*$^{\Delta Hep}$ mice were transplanted into *MUP-uPA* mice. Tumor multiplicity was assessed 6 months later ($n \geq 6$ mice/group).

(J) 10^4 HcPCs from 5-month-old DEN-treated WT mice were transplanted into either *MUP-uPA* or *MUP-uPA;Cd44*$^{-/-}$ hosts and tumor multiplicity was assessed 6 months later ($n \geq 3$ mice/group).

(K) *Cd44*$^{F/F}$ and *Cd44*$^{\Delta Hep}$ males were DEN-challenged and tumor multiplicity and size were determined 9 months later.

All bar graphs in (G–K) represent the mean ± SEM. **$p \leq 0.01$, ***$p \leq 0.001$; ns, not significant. See also Figure S1.

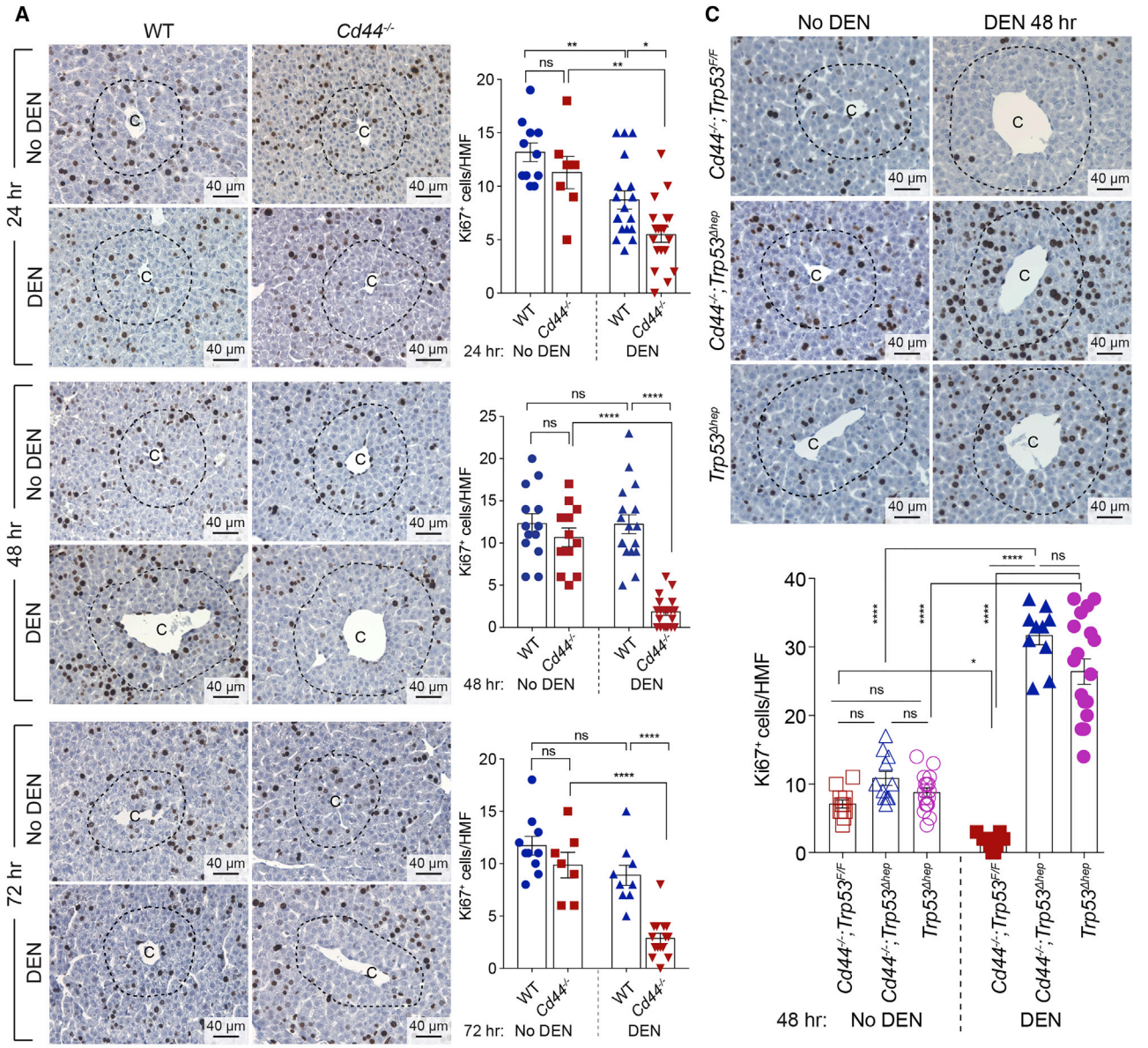

(legend on next page)

lesions and HCC nodules of both DEN-treated and *Tak1*$^{\Delta Hep}$ mice, where it is also expressed as CD44v6 (Figure 1A). Transformed hepatocytes in human HCC also express CD44, while CD44 expression in normal liver tissue is restricted to non-parenchymal cells (Figure 1B).

CD44 expression was significantly upregulated in human HCC with different etiologies and geographical origins (Figures 1C and 1D), available from a public database (www.ncbi.nlm.nih.gov/geo, GSE14323) of U.S. that were induced by hepatitis C virus (HCV) (Mas et al., 2009) (Figure 1C), and previous study conducted in France (Nault et al., 2013), that included HCC induced by alcohol consumption, hepatitis B virus (HBV), or HCV infections (Figure 1D and Table S1). *CD44* expression significantly correlated with both tumor grade (Figure 1E) and differentiation (Figure 1F). In a previous study, CD44 was shown to positively correlate with poor prognosis and reduced patient survival (Endo and Terada, 2000).

To test the role of CD44 in HCC initiation, we administered DEN to BL/6 (wild-type [WT]) and *Cd44*$^{-/-}$ mice where CD44 is absent in all cell types. *Cd44*$^{-/-}$ mice were largely resistant to HCC induction, not only tumor numbers and sizes but also tumor incidence was reduced in *Cd44*$^{-/-}$ mice (Figure 1G). Histologically, however, *Cd44*$^{-/-}$ tumors resembled WT tumors (Figure S1A). CD44 ablation in *Tak1*$^{\Delta Hep}$ mice (*Tak1*$^{\Delta Hep}$;*Cd44*$^{-/-}$) also reduced tumor burden but mostly affected tumor multiplicity rather than size (Figure 1H). Ki67 immunohistochemistry (IHC) showed fewer proliferating cells in the background liver and tumor nodules of *Tak1*$^{\Delta Hep}$;*Cd44*$^{-/-}$ mice than in *Tak1*$^{\Delta Hep}$ mice (Figure S1B).

CD44 Acts in the Hepatocyte Compartment

To determine whether CD44 acts in HcPCs, we isolated HcPCs from 8-week-old *Tak1*$^{\Delta Hep}$ and *Tak1*$^{\Delta Hep}$;*Cd44*$^{-/-}$ mice and transplanted them into 4-week-old *MUP-uPA* mice (Figure 1I). Young *MUP-uPA* mice express urokinase plasminogen activator (uPA) from a liver-specific major urinary protein (MUP) promoter and experience transient liver damage accompanied by compensatory proliferation, which makes them an ideal host for transplanted HcPCs (He et al., 2013). CD44-deficient HcPCs were compromised in their ability to generate HCC (Figure 1I). CD44, however, was not required within the host *MUP-uPA* liver for HcPC to HCC progression (Figure 1J). To further investigate hepatocyte-specific CD44 activities, we crossed *Cd44*$^{F/F}$ mice (Figure S1C) with Alb-*Cre* mice to generate *Cd44*$^{\Delta Hep}$ mice lacking CD44 in hepatocytes (Figure S1D). HCC multiplicity was significantly reduced in DEN-treated *Cd44*$^{\Delta Hep}$ mice (Figures 1K and S1E). Hence, the major site of CD44 action is the hepatocyte and/or HcPC, which originates from pericentral hepatocytes. Although under normal conditions hepatocytes do not express CD44, other liver cell types, including Kupffer cells, biliary epithelium, and lymphocytes, express CD44 (Flanagan et al., 1989). Since Kupffer cells can modulate tumor development, we examined whether CD44 ablation affected their abundance. Lack of CD44 either in hepatocytes (*Cd44*$^{\Delta Hep}$) or in all cell types (*Cd44*$^{-/-}$) did not affect macrophage recruitment into liver tumors (Figures S1F and S1G).

CD44 Antagonizes p53 and Prevents Cell-Cycle Exit of Proliferating Hepatocytes

To understand what makes *Cd44*$^{-/-}$ mice HCC refractory, we examined whether CD44 alters the response to DEN. The liver of a 15-day-old male mouse, in which a single DEN dose (25 mg/kg) is sufficient for HCC induction, is at an early developmental phase with ongoing hepatocyte proliferation. Ki67 IHC indicated that proliferating hepatocytes were distributed throughout the liver (Figures 2A and S2A). DEN is a procarcinogen that is activated by Cyp2E1 (Kang et al., 2007), an enzyme that is only expressed in pericentral hepatocytes, which are arranged in 6 to 7 layers around the central vein (Bahar Halpern et al., 2017) (also Figure S3A). Although the presence or absence of CD44 had no effect on hepatocyte proliferation in the unchallenged liver, DEN administration led to a marked decrease in proliferating pericentral hepatocytes in the *Cd44*$^{-/-}$ liver (Figures 2A and S2A). This effect was first detected 24 hr post-DEN and became more pronounced by 48 hr and 72 hr post-DEN. By contrast, DEN led to only marginal and transient suppression of pericentral hepatocyte proliferation in the WT mice only at 24 hr after its administration (Figures 2A and S2A). Given the known ability of p53 to block proliferation of damaged cells, we compared p53 induction in DEN-treated WT and *Cd44*$^{-/-}$ livers. DEN administration led to p53 induction within 6 hr in both WT and *Cd44*$^{-/-}$ mice (Figure 2B). Induction of p53 was confined to the pericentral region, and no obvious differences were observed between the two genotypes (Figure 2B). However, at 24 hr post-DEN, very little p53 staining was observed in the WT liver, while nuclear p53 remained abundant in the CD44-deficient pericentral zone. At 48 hr post-DEN, p53 was almost undetectable in the WT liver, while low amounts of nuclear p53 were still present in the CD44-deficient pericentral zone (Figure 2B).

To examine whether the cell-cycle exit of proliferating pericentral hepatocytes after DEN challenge is mediated by the p53 pathway, we generated *Trp53* and *Cd44* double-knockout mice (*Trp53*$^{\Delta Hep}$;*Cd44*$^{-/-}$) and used *Trp53*$^{F/F}$;*Cd44*$^{-/-}$ and *Trp53*$^{\Delta Hep}$ mice as controls. Ki67 IHC of livers from 15-day-old DEN-injected mice of these genotypes revealed that deletion of *Trp53* in hepatocytes prevented cell-cycle exit in DEN-challenged *Cd44*$^{-/-}$ livers (compare *Trp53*$^{F/F}$;*Cd44*$^{-/-}$ and *Trp53*$^{\Delta Hep}$;*Cd44*$^{-/-}$) (Figures 2C and S2B). Moreover, *Trp53* deletion significantly increased proliferation in the pericentral region (compare No DEN to DEN) (Figures 2C and S2B). However, as observed in the *Cd44*$^{-/-}$ liver (Figure 2A), DEN-challenged p53-sufficient *Trp53*$^{F/F}$;*Cd44*$^{-/-}$ pericentral hepatocytes exited the cell cycle as indicated by a decrease in Ki67^{+} pericentral cells (Figures 2C and S2B). No differences in the number of proliferating pericentral hepatocytes were observed prior to DEN administration (Figures 2C and S2B).

Figure 2. Proliferative Pericentral Hepatocytes Exit the Cell Cycle in Response to DNA Damage in the Absence of CD44

(A–C) Fifteen-day-old males of indicated genotypes were treated with ± DEN (25 mg/kg), and liver sections were stained with either Ki67 (A and C) or p53 (B) antibodies at indicated time points. The numbers of stained zone 3 cells per high magnification field (HMF) were determined (n ≥ 3 mice/group) (C, pericentral area; ND, not detectable). Student's t test was used to test the difference between two groups and one-way ANOVA with Tukey's multiple comparison test was used for more than two groups. All bar graphs represent the mean ± SEM. *p ≤ 0.05, **p ≤ 0.01, ****p ≤ 0.0001; ns, not significant. See also Figure S2.

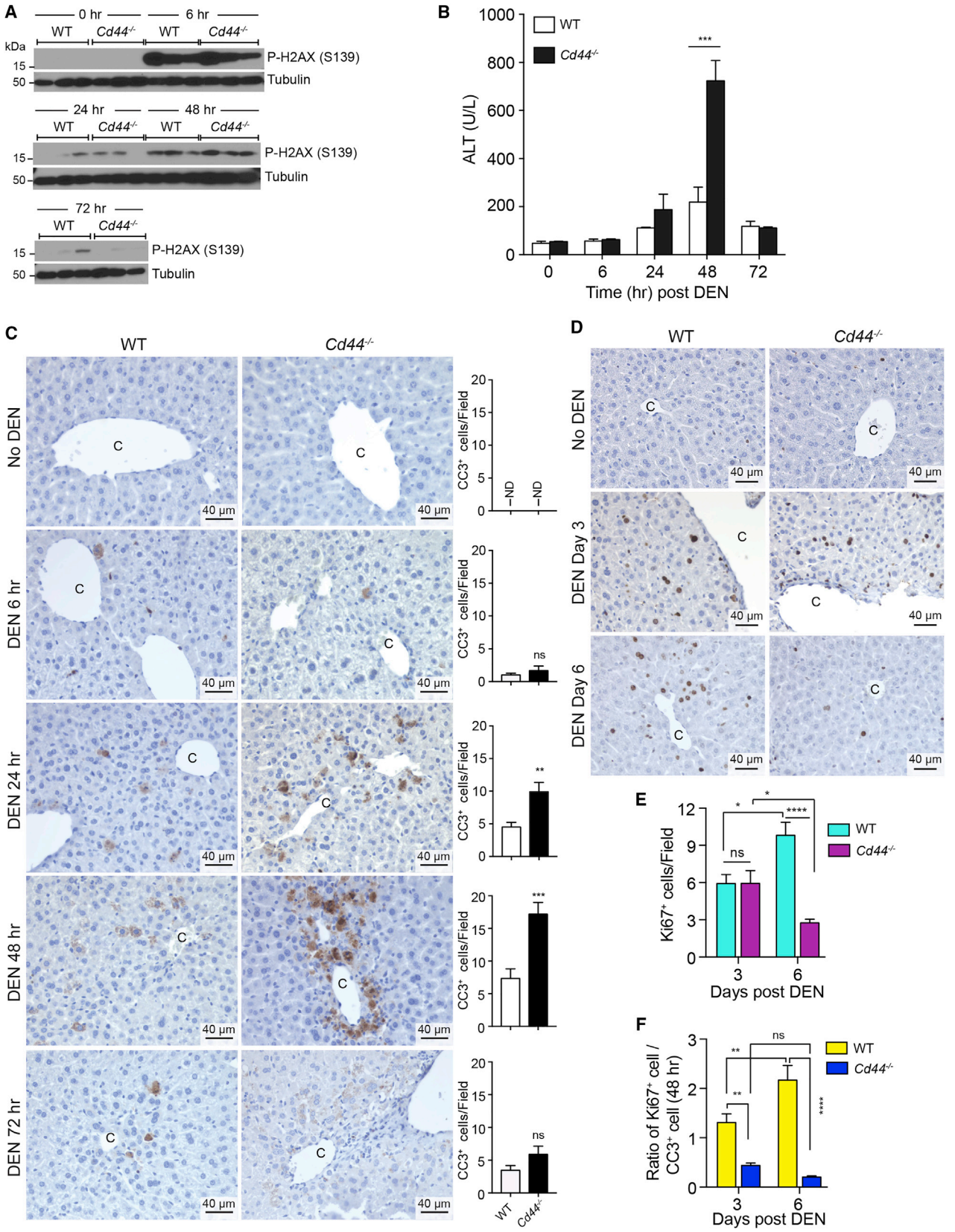

(legend on next page)

Adult hepatocytes are fully differentiated and rarely divide in the absence of liver damage (see below). In such mice, DEN challenge results in poor HCC induction, unless accompanied by a tumor promoter, such as phenobarbital or HFD (Park et al., 2010). Since CD44 is also required for tumor initiation in the non-synchronous *Tak1*$^{\Delta Hep}$ model, in which hepatocyte damage lasts for quite some time (Inokuchi et al., 2010), we examined the impact of CD44 on the DEN-induced damage response in 8- to 12-week-old mice. First, we compared the ability of DEN to undergo metabolic activation and induce DNA damage in the two genotypes. Induction of H2AX phosphorylation, a p53-independent indicator of the DNA damage response (Sharma et al., 2012), did not differ between WT and *Cd44*$^{-/-}$ livers (Figures 3A and S3A), indicating that CD44 has no effect on the ability of DEN to damage DNA. As expected, DNA damage was confined to the pericentral region, as indicated by Cyp2E1 and phospho-H2AX double-positive cells (Figure S3A). Despite the absence of genotype-specific differences in DNA damage, DEN administration led to much more liver damage, measured by alanine aminotransferase (ALT) release to the circulation, in *Cd44*$^{-/-}$ mice than in WT counterparts (Figure 3B). TUNEL (terminal deoxynucleotidyl transferase dUTP nick end labeling) assay (Figure S3B) and cleaved-caspase-3 (CC3) IHC (Figures 3C and S3C) confirmed these results and revealed that apoptosis in DEN-exposed livers was mainly confined to the pericentral zone, and was more substantial in the *Cd44*$^{-/-}$ liver. Enhanced DEN-induced apoptosis was also observed in *Cd44*$^{\Delta Hep}$ livers (Figure S3C), confirming that expression of CD44 in the hepatocyte compartment is important for averting cell death in response to DNA damage.

Previous studies have indicated that increased hepatocyte death corresponds to enhanced compensatory proliferation, which correlates with augmented liver tumorigenesis (Maeda et al., 2005). In 8- to 12-week-old WT and *Cd44*$^{-/-}$ livers, quiescent pericentral hepatocytes enter the cell cycle by 72 hr post-DEN (after cell death has peaked at 48 hr) as indicated by Ki67^{+} staining (Figures 3D and 3E). The difference in hepatocyte proliferation between WT and *Cd44*$^{-/-}$ livers was much more apparent at 6 days post-DEN (Figure 3E). Even though the average number of Ki67^{+} hepatocytes at 72 hr post-DEN was similar in WT and *Cd44*$^{-/-}$ livers (Figures 3D and 3E), when normalized to the cell death index, compensatory proliferation was considerably reduced in the *Cd44*$^{-/-}$ liver (Figure 3F). While the compensatory proliferation-to-death ratio in the WT liver was just over 1, suggesting that for every hepatocyte that died at 48 hr, at least one hepatocyte entered the cell cycle at 72 hr, in the *Cd44*$^{-/-}$ liver this ratio was 0.5, suggesting inefficient cell-cycle entry (Figure 3F). The ratio further increased to >2 at day 6 in the WT liver, while *Cd44*$^{-/-}$ hepatocytes remained non-proliferative (Figure 3F).

We examined whether CD44 also affected p53 induction in the non-proliferating hepatocytes of 8- to 12-week-old mice. As seen in young mice, DEN administration led to rapid p53 induction in older mice, which was not affected by the CD44 status (Figures 4A and 4B). The induced p53 was phosphorylated at Serine (S) 15 (Figure 4B), suggesting it was active. However, little nuclear p53 remained in WT livers at 48 hr post-DEN, whereas nuclear p53 was still plentiful in *Cd44*$^{-/-}$ and *Cd44*$^{\Delta Hep}$ livers (Figures 4A, S4A, and S4B). At 72 hr post-DEN, the residual p53 in the WT liver was mostly cytosolic (with some areas of weak nuclear signal), indicative of its inactivation, but in the *Cd44*$^{-/-}$ liver p53 remained nuclear (Figure 4A). Of note, p53 nuclear accumulation was confined to zone 3 (Figure S4A) and its sustained expression in the CD44-deficient liver was confirmed by immunoblotting (IB) analysis (Figure 4B). Nuclear p53 accumulation was accompanied by induction of p53 targets: *Cdkn1 (p21*^{Waf1}*)*, *Pmaip1* (*Noxa)*, and *Bbc3* (*Puma)* (Figures 4C, S4C, and S4D). Remarkably, enhanced p53 target gene expression in the *Cd44*$^{-/-}$ liver was already apparent at 6 hr post-DEN and was confirmed by qRT-PCR and IB analysis (Figures 4C and S4D), suggesting that p53 transcriptional activity was enhanced in the absence of CD44. By contrast, CD44 deficiency had no effect on p53 mRNA levels (Figure S4D).

Enhanced p53 Activity Inhibits Hepatic Carcinogenesis

To examine the role of p53 in DEN-induced hepatocyte death and HCC initiation, *Trp53*$^{\Delta Hep}$*;Cd44*$^{-/-}$ and *Cdkn1*$^{-/-}$*;Cd44*$^{-/-}$ double-knockout mice, and *Trp53*$^{F/F}$*;Cd44*$^{-/-}$, *Trp53*$^{\Delta Hep}$, and *Cdkn1*$^{-/-}$ control mice were DEN-challenged. Absence of either p53 or p21^{Waf1} in the *Cd44*$^{-/-}$ background prevented the increase in liver damage (Figure 4D) and restored DEN-induced hepatic carcinogenesis (Figure 4E). Malignancy markers in both *Trp53*$^{\Delta Hep}$ and *Trp53*$^{\Delta Hep}$*;Cd44*$^{-/-}$ tumors were upregulated compared with WT and *Cd44*$^{-/-}$ tumors (Figure S4E). Not only did *p53* deletion on a WT background enhance *Cd44* expression and other malignancy markers (compare WT with *Trp53*$^{\Delta Hep}$), its deletion in the *Cd44*$^{-/-}$ background (compare *Cd44*$^{-/-}$ with *Trp53*$^{\Delta Hep}$*;Cd44*$^{-/-}$) restored expression of malignancy markers that were suppressed in *Cd44*$^{-/-}$ tumors (Figure S4E). These results suggest that p53 activation, which is extended in the absence of CD44, not only promotes cell-cycle exit or death of DNA-damaged hepatocytes in young and adult mice, respectively, but also affects the conversion of DNA-damaged and presumably initiated zone 3 hepatocytes into HcPCs. These conclusions are consistent with other studies showing that p53 induces apoptotic elimination of genomically damaged cells (Fridman and Lowe, 2003) and also blocks reprogramming of fibroblasts into induced pluripotent stem cells (Hong et al., 2009).

CD44 Is Required for Mdm2 Nuclear Translocation and Akt Activation

Mdm2 inhibits p53 transcriptional activity and enhances its degradation (Michael and Oren, 2002; Shi and Gu, 2012). We

Figure 3. CD44 Inhibits Killing of DEN-Exposed Adult Pericentral Hepatocytes

(A–F) Eight- to 12-week-old WT and *Cd44*$^{-/-}$ males were DEN-challenged (100 mg/kg). Livers and serum were collected when indicated and analyzed as shown. (A) Liver lysates were IB-analyzed with the indicated antibodies. (B) Serum ALT was measured (n = 3). (C) CC3 IHC and quantification (n ≥ 8 different fields from three different mice for each time point). (D and E) Ki67 IHC (D) and quantification of Ki67^{+} hepatocytes (E). (F) Compensatory proliferation index was calculated by dividing the average number of Ki67^{+} hepatocytes at days 3 and 6 from (E) by the number of CC3^{+} hepatocytes from (C) at 48 hr post-DEN (n ≥ 6 different fields from three different mice for each time point). All bar graphs represent the mean ± SEM. C, pericentral area; ND, not detectable. *p ≤ 0.05, **p ≤ 0.01, ***p ≤ 0.001, ****p ≤ 0.0001; ns, not significant. See also Figure S3.

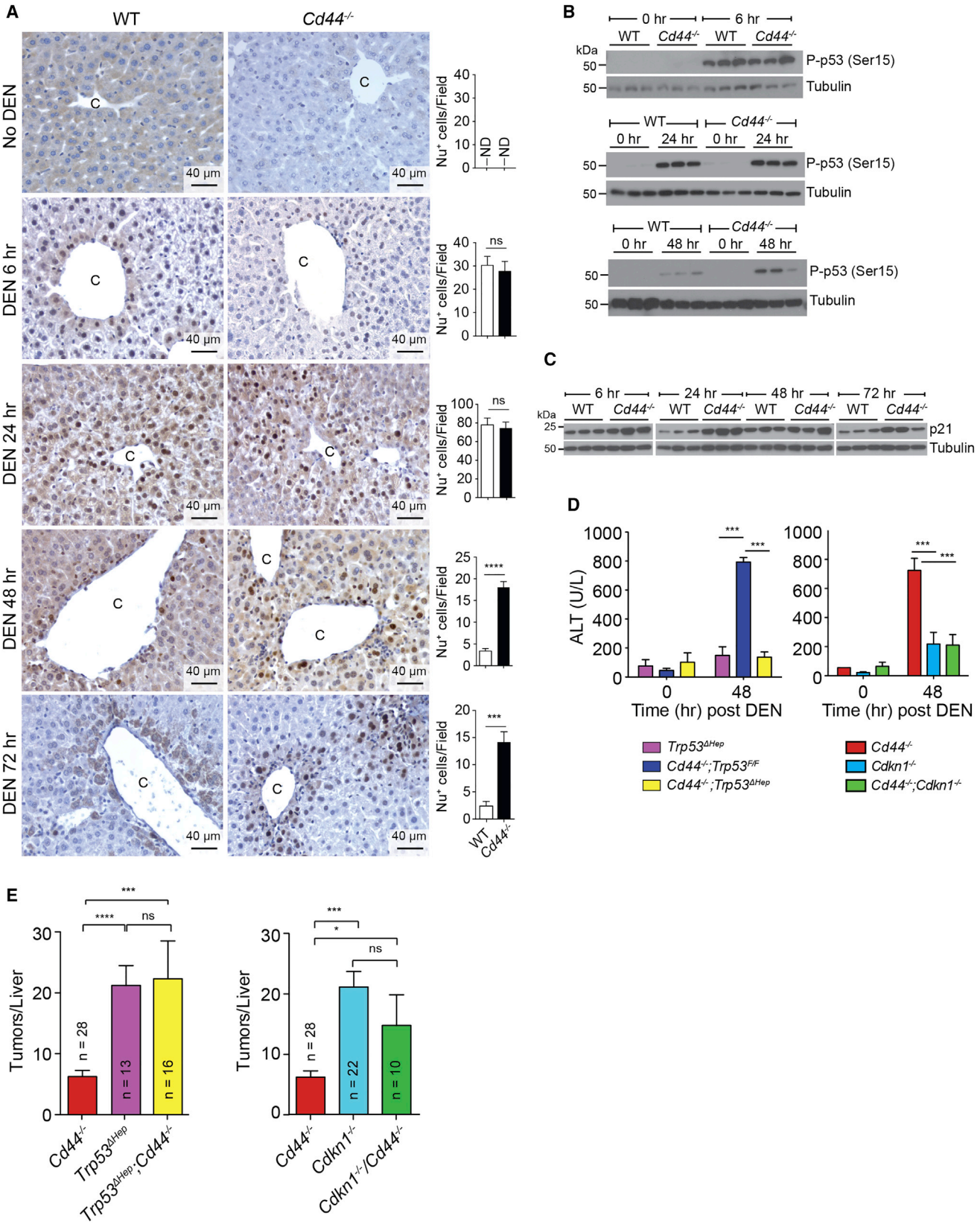

(legend on next page)

examined whether CD44 influences Mdm2 expression. IHC analysis revealed that DEN exposure led to Mdm2 induction in both WT and *Cd44*$^{-/-}$ livers, but while WT hepatocytes accumulated nuclear Mdm2, *Cd44*$^{-/-}$ hepatocytes showed cytoplasmic Mdm2 accumulation, which peaked at 48 hr post-DEN (Figures 5A and S5A). Similar results were obtained in *Cd44*$^{\Delta Hep}$ mice, which showed cytoplasmic Mdm2 accumulation (Figure S5B). We prepared liver whole-cell lysate (WCL), as well as cytosolic and nuclear fractions and examined Mdm2 expression (Figure S5C). While there was no difference in total Mdm2 between WT and *Cd44*$^{-/-}$ WCL, there was clear cytoplasmic retention of Mdm2 in the *Cd44*$^{-/-}$ liver with lower amounts of nuclear Mdm2 (Figure S5C). Notably, the peak in Mdm2 cytosolic retention coincided with the peak in hepatocyte death at 48 hr post-DEN (Figures 3B and 3C). In both WT and CD44-deficient mice, Mdm2 induction after DEN challenge was confined to the pericentral zone, the same area at which p53 was induced. *In situ* hybridization (ISH) analysis confirmed that DEN treatment led to induction of *Mdm2* mRNA in pericentral hepatocytes of both WT and *Cd44*$^{-/-}$ mice (Figure S5D). qRT-PCR analysis revealed no difference in *Mdm2* mRNA induction between the two strains (Figure S5E).

Nuclear translocation of Mdm2 in cell lines was shown to be controlled by phosphorylation of S166/186, which reside within an Akt phosphorylation motif: RXRXXS/T (Mayo and Donner, 2001; Zhou et al., 2001). Treatment of murine HCC cell line Dih10 with cisplatin activated Akt (phosphorylation at S473) and increased both total and nuclear amounts of phospho-S166 Mdm2 (Figure S5F). Inhibition of Akt in cisplatin-treated Dih10 cells with the pan-Akt inhibitor MK2206 reduced the amounts of phospho-S166 Mdm2 without affecting total Mdm2 (Figure S5F). However, nuclear Mdm2 and phospho-S166 Mdm2 were reduced (Figure S5F), indicating that Akt activation may also be involved in Mdm2 nuclear translocation in hepatocytes and HCC cells. Treatment of Dih10 cells with cisplatin alone upregulates several p53 target genes, as expected, but Akt inhibition further increased p53 target gene expression (Figure S5G). p53 mRNA itself was not affected. To validate the effect of Akt inhibition on p53 targets, we treated Dih10 cells with the Mdm2 inhibitor and p53 activator Nutlin-3 (Vassilev et al., 2004). Nutlin-3 treatment further increased cisplatin-induced p53 target gene expression (Figure S5H), suggesting that even though the mechanisms of action of Akt inhibitors differ from that of Nutlin-3, they both potentiate p53 activity. We therefore examined the status of Akt activation in DEN-treated WT versus *Cd44*$^{-/-}$ livers. Indeed, IHC analysis of liver sections revealed that DEN treatment led to Akt activation in pericentral hepatocytes of WT liver but not in *Cd44*$^{-/-}$ or *Cd44*$^{\Delta Hep}$ livers (Figures 5B and S5B). IB analyses confirmed absence of Akt activation in *Cd44*$^{-/-}$ livers (Figure S5I). Moreover, nuclear phospho-S166 Mdm2 was much lower in DEN-treated *Cd44*$^{-/-}$ livers compared with DEN-treated WT livers (Figure 5C). Furthermore, treatment of WT mice with the pan-Akt inhibitor blocked nuclear translocation of phospho-S166 Mdm2 and resulted in cytosolic retention of the non-phosphorylated protein after DEN treatment (Figure 5D). As a consequence, nuclear p53 was elevated in MK2206-treated mice (Figure 5D). Moreover, we found a positive correlation between CD44 expression and phospho-S166 Mdm2 levels in human HCC tissues (Figure 5E), validating our findings in mice.

CD44 Is Required for EGFR Activation in Pericentral Hepatocytes

CD44 interacts with growth factor receptors, including EGFR and c-Met (Ponta et al., 2003), both of which are needed for optimal liver regeneration (Huh et al., 2004; Natarajan et al., 2007). Either receptor can activate Akt, although EGFR is not as effective as other ErbB family members (Soltoff et al., 1994), suggesting that EGFR might need a cofactor for efficient signaling to Akt. Using IHC, we found that EGFR was phosphorylated throughout the WT liver within 3 hr of DEN injection (Figure 6A), which is consistent with the previously observed induction of EGFR ligands after DEN challenge (Lanaya et al., 2014; Maeda et al., 2005). Strikingly, no EGFR phosphorylation was detected in the pericentral zone of CD44-deficient livers (both *Cd44*$^{-/-}$ and *Cd44*$^{\Delta Hep}$) as early as 3 hr after DEN challenge (Figures 6A and 6B). Interestingly, the periportal region of CD44-deficient livers showed EGFR phosphorylation, although downstream effectors such as Akt were not activated in this region. This peculiar requirement of CD44 for EGFR activation only at the pericentral zone was not due to differential EGFR expression across the portal-central hepatocyte differentiation gradient (Figures 6B and 6C). IB analysis of isolated hepatocytes 3 hr post-DEN confirmed the defect in EGFR activation in *Cd44*$^{-/-}$ cells (Figure 6D).

To determine whether EGFR activation was involved in regulation of Mdm2 subcellular distribution and p53 expression, we deleted EGFR in *Egfr*$^{F/F}$*;Mx1-Cre* mice (*Egfr*$^{\Delta Mx}$) using poly (I:C) injection (Figure S6A) and challenged *Egfr*$^{F/F}$ and *Egfr*$^{\Delta Mx}$ mice with DEN. Notably, EGFR ablation had the same effect on Mdm2 and p53 expression as CD44 ablation: Mdm2 was mainly cytoplasmic 48 hr after DEN challenge in *Egfr*$^{\Delta Mx}$ mice while it was nuclear in *Egfr*$^{F/F}$ mice (Figure 6E). Correspondingly, pericentral p53 expression (Figure 6E), caspase-3 activation (Figure S6A), and serum ALT (Figure S6B) were higher in DEN-challenged *Egfr*$^{\Delta Mx}$ liver than in the *Egfr*$^{F/F}$ liver. EGFR ablation also inhibited Akt activation (Figure S6A). Blocking EGFR signaling in WT mice with Gefitinib prevented EGFR activation and consequently blocked Akt activation as indicated by IB analyses (Figure S6C). Gefitinib treatment resulted in Mdm2 cytoplasmic retention as well as p53 and caspase-3 hyperactivation 48 hr after DEN injection (Figure S6D). Downstream p53 targets such as p21^{Waf1} and PUMA were also increased upon Gefitinib treatment in WT livers (Figure S6E). EGFR inhibition in *Cd44*$^{-/-}$ mice,

Figure 4. Impaired Termination of the p53 Response in the Absence of CD44

(A–D) 8-12-week-old male mice of indicated genotypes were DEN-challenged (100 mg/kg). Livers and sera were collected when indicated and analyzed: (A) p53 IHC. Bar graphs on the right show number of hepatocytes with nuclear p53 per field ($n \geq 7$ different fields from three different mice for each time point; C, pericentral area). (B and C) IB analysis of liver lysates probing phospho-S15 p53 (B) and p21 (C). (D) Serum ALT ($n = 3$ mice for each genotype per time point). (E) Fifteen-day-old male mice of indicated genotypes were DEN-challenged (25 mg/kg) and tumor multiplicity was assessed 9 months later.

All bar graphs represent the mean ± SEM. *$p \leq 0.05$, ***$p \leq 0.001$, ****$p \leq 0.0001$; ns, not significant. See also Figure S4.

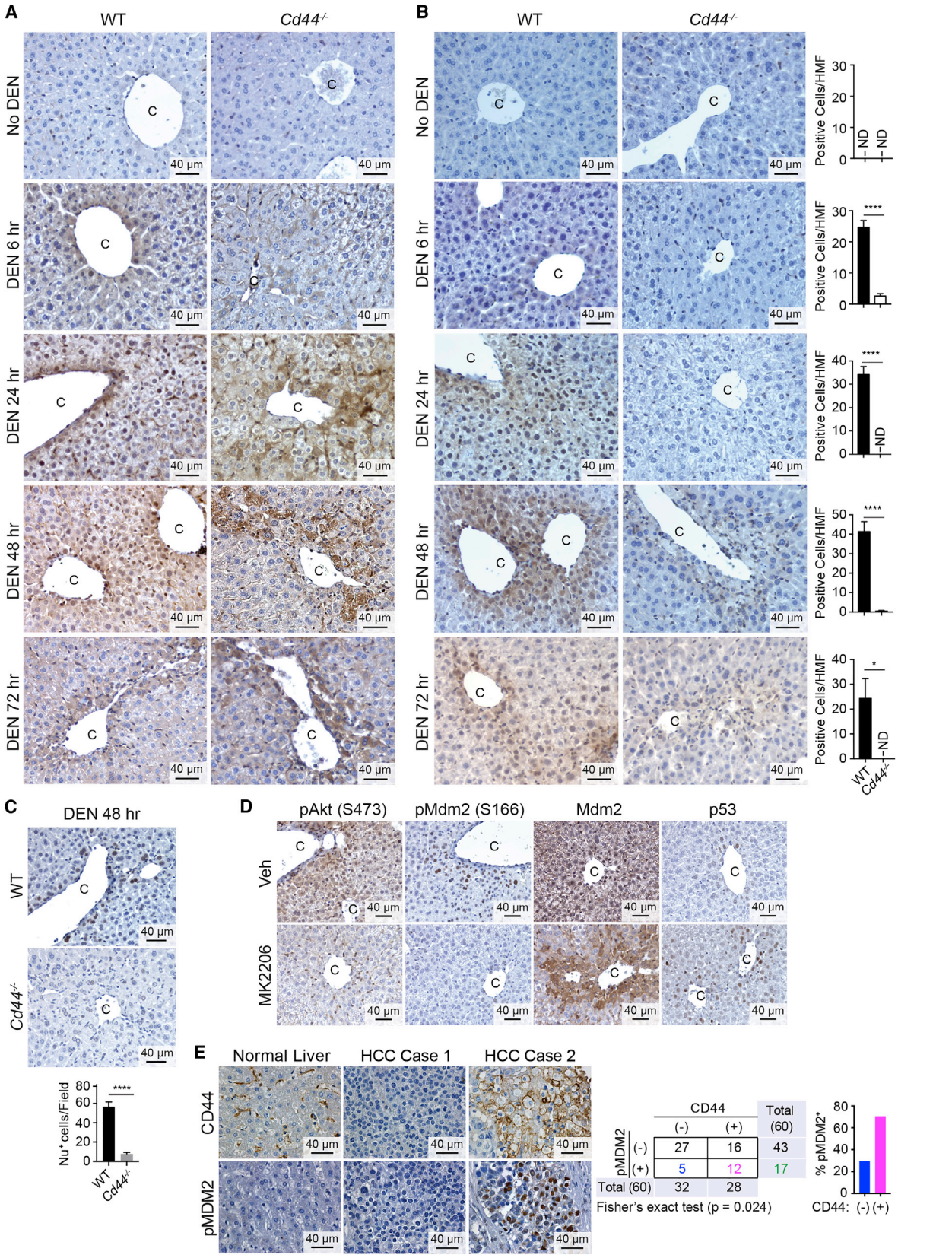

(legend on next page)

however, did not further augment p53 activation (Figures S6E and S6F), indicating that the enhanced p53 response in *Cd44*$^{-/-}$ livers is likely due to defective DEN-stimulated EGFR signaling.

Control of CD44 Expression

The above experiments indicate that CD44 acts in pericentral hepatocytes to control EGFR and Akt activation and promote nuclear shuttling of Mdm2 in the first 24 hr after DEN administration. This requires CD44 expression in DEN-metabolizing zone 3 hepatocytes. Indeed, ISH confirmed that DEN administration induced *Cd44* mRNA in the pericentral zone (Figure 7A). Time course studies revealed *Cd44* mRNA induction as early as 3 hr after DEN injection (Figure 7B), indicating that *Cd44* expression coincides temporally and spatially with the CD44-dependent signaling events described above. β-catenin/TCF4 was shown to control *Cd44* expression (Wielenga et al., 1999). However, whether β-catenin/TCF4-mediated *Cd44* expression is direct or indirect is not clear (https://web.stanford.edu/~rnusse/pathways/targets.html). To identify whether β-catenin activation upregulates *CD44* in human HCC, we compared *CD44* transcript levels in HCCs with or without activating β-catenin mutations (Nault et al., 2013) (Table S1). Human *CD44* mRNA expression was not influenced by the β-catenin status (Figure S7A).

To identify additional transcription factors that might control *Cd44* expression in hepatocytes and HCC cells, we examined the *Cd44* promoter for *cis*-acting elements and found several putative STAT3 binding sites, along with recognition sites for other transcription factors. STAT3 is activated within 4 hr after DEN injection, paralleling induction of interleukin (IL)-6, a strong STAT3 activator (Maeda et al., 2005; Sakurai et al., 2008). Moreover, an autocrine IL-6-STAT3 loop controls HcPC generation (He et al., 2013). We therefore investigated whether IL-6-STAT3 signaling contributes to *Cd44* induction. Stimulation of isolated primary hepatocytes with IL-6 induced *Cd44* mRNA expression (Figure S7B). The HCC cell lines Dih10 and DihXY express varying amounts of CD44 (Figure S7C). Chromatin immunoprecipitation (ChIP) performed on DihXY cells under normal culture conditions showed STAT3 enrichment at the *Cd44* promoter, which was diminished after serum starvation (Figure 7C). To activate STAT3, we stimulated serum-starved cells with IL-6 and performed ChIP on the *Cd44* promoter. IL-6 treatment resulted in STAT3 enrichment at the *Cd44* promoter in both cell lines (Figures 7D and S7D). Additionally, primary hepatocytes isolated 6 hr after DEN also showed STAT3 recruitment on the *Cd44* promoter (Figure S7E), despite the fact that isolation of total hepatocytes results in dilution of CD44-expressing pericentral hepatocytes with CD44-negative zone 1 and 2 cells. Consistent with these results, inhibition of JAK1/2, the upstream kinases responsible for STAT3 activation, with a pharmacological inhibitor (AZD1480) suppressed both STAT3 activation (Figure 7E) and *Cd44* transcription (Figure 7F). To evaluate the role of IL-6 in *CD44* expression in human tumors, we measured *CD44* transcript levels in hepatocellular adenomas (HCAs) harboring activating IL-6 signal transducer (*IL6ST; GP130*) mutations (Pilati et al., 2014). In accordance with our findings, we found significant upregulation of *CD44* mRNA expression in *IL6ST* mutated tumors (Figure 7G).

DISCUSSION

While some cancers, such as colorectal cancer, may be derived from continuously cycling cells (Vries et al., 2010), HCC, both DEN- and steatohepatitis-induced, is initiated by differentiated, zone 3 hepatocytes (Font-Burgada et al., 2015). How a single, differentiated cell goes on to acquire the minimal set of oncogenic mutations that is needed for its conversion to a malignant CIC despite the existence of potent tumor-suppressive mechanisms is unknown and remains a main hindrance toward full understanding of tumor initiation. Since most mutations are introduced as a result of DNA damage (Hoeijmakers, 2009), the ability of the DNA-damaged cell to divide, copy the first oncogenic mutation into the complementary DNA strand, and transmit the mutated sequences to its progeny is particularly puzzling given that DNA damage results in p53 activation, which causes cell-cycle exit, prevents cell-cycle entry, or induces apoptosis. Even in proliferating cells, endogenous p21^{Waf1} controls the commitment to cell cycle by titrating mitogen-induced cyclin-dependent kinase 2 activity (Spencer et al., 2013). Although this important competition was shown to take place in tissue culture cells, it is difficult to envision how such a process can take place within fully differentiated cells, such as pericentral hepatocytes. Our results show that CD44, one of the ubiquitous CSC markers (Zoller, 2011), plays a critical role in tumor initiation and allows growth factor signaling to override the DNA damage response, thereby tipping the balance toward cell survival and proliferation. Exposure of differentiated hepatocytes to the alkylating intermediate generated by DEN metabolism results in the DNA damage response that leads to induction of p53 and its target genes, including *Cdkn1* (Lane and Levine, 2010). DEN also triggers a necroinflammatory response that is initiated by release of IL-1 and other DAMPs and culminates in NF-κB and STAT3 activation (He et al., 2010; Maeda et al., 2005; Sakurai et al., 2008). DEN metabolites cause oncogenic mutations, for instance the *Braf*^{V637E} mutation (He et al., 2013), whereas STAT3 activation induces CD44 expression in pericentral hepatocytes, the very cells in which DEN undergoes metabolic activation (Kang et al., 2007). Using both young and adult mice we

Figure 5. CD44 Is Required for Optimal Akt Activation and Mdm2 Nuclear Translocation

(A–C) WT and *Cd44*$^{-/-}$ males (8- to 12-week-old) were DEN-challenged (100 mg/kg), their livers were collected when indicated and IHC-analyzed for Mdm2 (A), phospho-S473 Akt (B), and phospho-S166 Mdm2 (C). Bar graphs show number of hepatocytes positive for indicated proteins ($n \geq 6$ different fields from three different mice for each time point; mean ± SEM).

(D) WT mice were treated with Veh or MK2206 (100 mg/kg/day) starting 1 day prior to DEN challenge (100 mg/kg). Livers were collected 48 hr later and IHC-analyzed with the indicated antibodies ($n \geq 3$ mice/group).

(E) Human HCC tissue array was IHC-analyzed for CD44 and phospho-S166 MDM2 co-expression in parallel sections. Number of samples positive or negative for each protein is indicated in the table and the graph indicates the percent of total pMDM2^{+} samples that is either positive or negative for CD44.

(C = central vein).

*$p \leq 0.05$, ****$p \leq 0.0001$. See also Figure S5.

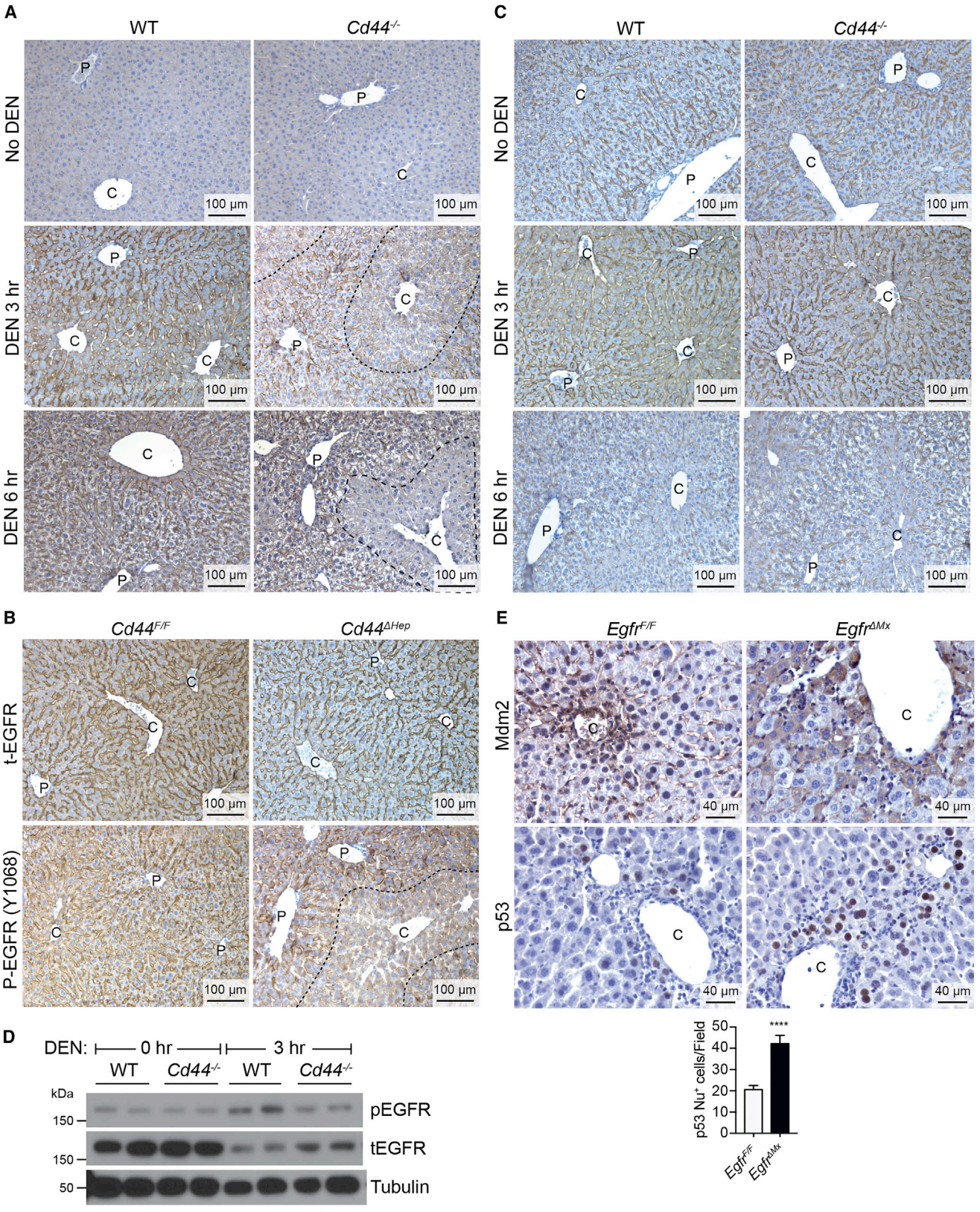

(legend on next page)

established that although initiation of the p53 response is not affected by CD44, its termination is CD44-dependent. Compared with the higher dose of DEN (100 mg/kg) used in adult mice, activation of p53 by the lower DEN dose (25 mg/kg) used to induce HCC in young mice does not induce extensive hepatocyte death. Instead, in 2-week-old mice in which most hepatocytes are still cycling, p53 activation mainly results in the cell-cycle exit of *Cd44*$^{-/-}$ pericentral hepatocytes. By contrast, transient p53 induction hardly affects the proliferation of WT pericentral hepatocytes, which go on to accumulate the critical set of oncogenic mutations needed for their conversion to HcPCs. The higher DEN dose used in adult mice activates p53 to a greater extent than the dose used in young mice, resulting in hepatocyte death and a limited amount of compensatory proliferation, that due to its transient nature, is insufficient for HCC induction unless accompanied with a tumor promoter (Maeda et al., 2005). However, even this limited amount of compensatory proliferation is severely compromised by the absence of CD44, which inhibits HCC initiation not only in young DEN-challenged mice but also in *Tak1*$^{\Delta hep}$ mice in which liver damage persists throughout adult life (Bettermann et al., 2010; Inokuchi et al., 2010).

By promoting Mdm2 nuclear translocation and terminating the p53 response, CD44 prevents the premature cell-cycle exit and death of pericentral hepatocytes that had acquired a potential oncogenic mutation in at least one DNA strand and allows them to proliferate, duplicate the mutation, and transmit it to one of their progeny, which need to keep dividing in order to accumulate additional mutations. Since CD44 induction is controlled by IL-6 and it potentiates growth factor receptor tyrosine kinase signaling, it provides a means for mitogens to overcome the anti-proliferative effect of the DNA damage response, which is mediated by p21^{Waf1} (Spencer et al., 2013), whose ablation eliminates the requirement for CD44. Given the known ability of p53 to block the reprograming process responsible for generation of pluripotent stem cells (Hong et al., 2009), prolonged CD44 expression may also promote the conversion of initiated pericentral hepatocytes into HcPCs, whose transcriptomic profile resembles that of bile duct-derived bipotential hepatobiliary progenitors (He et al., 2013). These conclusions and hypotheses are summarized in Figure 7H.

CD44 is upregulated in human HCCs and its expression correlates positively with higher histological grades and poor differentiation. But when and how CD44 exerts its pro-tumorigenic function was heretofore completely unknown. Previous studies showing that p53 exerts its tumor-suppressive activity in breast epithelial cells through repression of *CD44* transcription (Godar et al., 2008), suggested that CD44 might play a critical role in tumor initiation. Now we show that CD44, whose expression is induced by STAT3, controls tumor initiation by terminating the p53-mediated DNA damage response. The critical pro-tumorigenic activity of CD44 is exerted through potentiation of EGFR (and probably c-Met) signaling in pericentral hepatocytes, the very cells within which DEN undergoes metabolic activation. Although previous studies have demonstrated the interaction of pan-CD44 and CD44v6 with EGFR and c-Met, respectively (Ponta et al., 2003), this was never shown to be critical for tumor initiation or even tissue repair. DEN administration and liver damage induce the expression of numerous EGFR ligands, including EGF, HB-EGF, epiregulin, betacellulin, and transforming growth factor α, as well as the c-Met ligand hepatocyte growth factor (HGF), most of which are mainly expressed by liver macrophages (Fuchs et al., 2014; Lanaya et al., 2014; Maeda et al., 2005). However, the zonal distribution of these ligands and their differential ability to stimulate EGFR and c-Met phosphorylation and signaling remain to be investigated. Nonetheless, it should be noted that EGFR is an inefficient activator of phosphatidylinositol 3-kinase (PI3K)-AKT signaling relative to c-Met or other growth factor receptors (Soltoff et al., 1994). Furthermore, CD44 was shown to recruit the adaptor LARG (Leukemia-Associated RhoGEF) into the EGFR signaling complex, thereby facilitating phosphoinositide production and Akt activation (Bourguignon, 2008). Thus, our findings provide an explanation for the focal, EGFR-dependent, activation of Akt in pericentral hepatocytes, which is important for induction of Mdm2 nuclear translocation. Of note, many different chemicals and xenobiotics, including carbon tetrachloride and alcohol, are metabolically activated in pericentral hepatocytes to cause centrilobular damage (Cederbaum, 2012), where CD44 signaling might also counteract p53 to prevent cell death and promote tumorigenesis.

DEN administration induces *Cd44* mRNA only in pericentral hepatocytes. *Cd44* expression is induced by IL-6 and ChIP experiments confirm recruitment of STAT3 to the *Cd44* promoter. Consequently, inhibition of STAT3 using a JAK1/2 inhibitor prevented *Cd44* induction. Given the known ability of DEN to induce IL-6 expression and STAT3 activation (He et al., 2010; Maeda et al., 2005), it is likely that the same factors contribute to *Cd44* induction and overcome the repressive activity of p53. Congruently, human liver tumors with activating *IL6ST/GP130* mutations (that activate STAT3) overexpress *CD44*. IL-6 trans-signaling is a critical factor for HCC development (Bergmann et al., 2017) and it is therefore plausible that either autocrine or paracrine IL-6 signaling keeps *CD44* expression elevated in HcPCs and established HCC nodules. The IL-6/JAK/STAT3 signaling axis, therefore, provides multiple potential targets for HCC therapy. In summary, CD44 couples the necroinflammatory response that leads to STAT3 activation to inhibition of the tumor-suppressive p53 response (Figure 7H). Obviously, this elaborate regulatory system did not evolve to control cancer initiation. Most likely, induction of CD44 expression in pericentral hepatocytes ensures growth factor-induced regeneration of these critical drug-metabolizing cells after acute toxic injury.

EGFR is overexpressed in 40% to 70% of human HCC (Buckley et al., 2008). EGFR antagonists had shown efficacy in rodent models of HCC (Fuchs et al., 2014), but were not too effective in

Figure 6. CD44-Dependent EGFR Activation in Pericentral Hepatocytes

(A–E) Eight- to 12-week-old male mice of indicated genotypes were DEN-challenged (100 mg/kg) and their livers were collected when indicated. (A) Stained for phospho-Y1068 EGFR. (B) *Cd44*$^{F/F}$ and *Cd44*$^{\Delta Hep}$ livers were IHC-analyzed with indicated antibodies at 3 hr post-DEN. (C) WT and *Cd44*$^{-/-}$ livers were stained for total EGFR. (D) Hepatocytes were isolated 3 hr post-DEN, and IB-analyzed with indicated antibodies. (E) Livers were collected 48 hr after DEN treatment and IHC-analyzed for Mdm2 and p53 ($n \geq 15$ different fields from ≥ 3 different mice/group; mean ± SEM). "C" = pericentral and "P" = periportal areas. ****$p \leq 0.0001$. See also Figure S6.

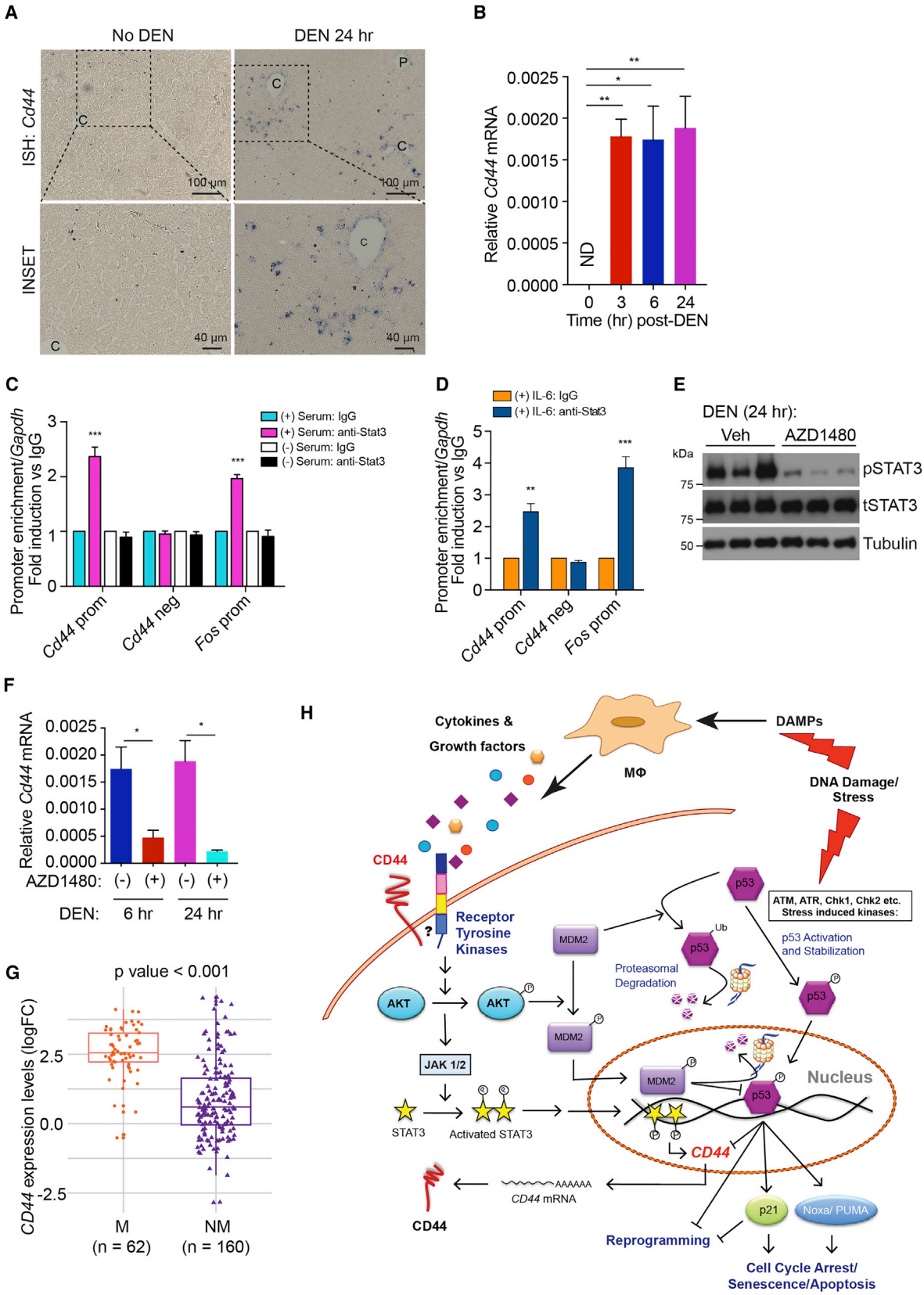

(legend on next page)

advanced human HCC. Our results suggest that CD44 targeting agents may enhance the efficacy of EGFR inhibitors and even lower the therapeutic dose for HCC treatment. Inducible *Egfr* ablation, which reduces HCC induction by DEN + phenobarbital (Lanaya et al., 2014) or treatment with an EGFR inhibitor, exerted the same effect on Mdm2 subcellular distribution and p53 as CD44 ablation. However, whereas CD44 is expressed and acts only in pericentral hepatocytes, EGFR is broadly expressed throughout the liver, including macrophages. Indeed, when EGFR is specifically deleted only in hepatocytes, DEN + phenobarbital administration results in enhanced liver damage and enhanced compensatory proliferation in response to growth and repair factors, whose production by liver macrophages is EGFR-dependent (Lanaya et al., 2014).

Our results indicate that inhibition of p53 accumulation and activity is a key early step in HCC initiation, which takes place long before p53-inactivating mutations are acquired. As discussed above, inhibition of p53 signaling is manifested in the very group of cells that give rise to HcPCs. Our findings demonstrate that CD44 antagonizes p53 by potentiating the Akt-stimulated nuclear translocation of Mdm2. Without CD44 or Mdm2, excessive p53 activation results in sustained induction of $p21^{Waf1}$, Noxa, and Puma. Although it has been difficult to identify the critical p53 target genes that mediate its tumor-suppressive activity (Aubrey et al., 2016), it was suggested that p53-mediated tumor suppression in breast cancer depends on repression of *CD44* transcription (Godar et al., 2008). Our results suggest that p53-mediated suppression of HCC initiation is dependent on $p21^{Waf1}$ induction. Expression of $p21^{Waf1}$ was also reported to be sufficient to halt the cell cycle in postnatal developing hepatocytes in unchallenged liver (Wu et al., 1996). Although in most cell types $p21^{Waf1}$ inhibits cell-cycle progression, under certain circumstances it also contributes to cell death (Gartel and Tyner, 2002). This seems to be the case in adult hepatocytes exposed to a high dose of DEN, whose death is prevented upon either p53 or $p21^{Waf1}$ ablation. Thus, prolonged p53 and $p21^{Waf1}$ induction in pericentral hepatocytes prevents acquisition of mutations and leads to the cell-cycle exit or death of DNA-damaged cells, and may also prevent the conversion of initiated hepatocytes into more proliferative HcPCs. These findings suggest that CD44 inhibitors, or antibodies that block their interaction with growth factor receptors, may be useful for preventing HCC development in chronically damaged and inflamed liver.

STAR★METHODS

Detailed methods are provided in the online version of this paper and include the following:

- KEY RESOURCES TABLE
- CONTACT FOR REAGENT AND RESOURCE SHARING
- EXPERIMENTAL MODEL AND SUBJECT DETAILS
  - Mice
  - Cell Lines
  - Primary Cells
  - Human Samples and Study Approval
- METHOD DETAILS
  - Cell Culture and *In Vitro* Treatments
  - *In Vivo* Treatments
  - Nuclear-Cytoplasmic Extraction and Immunoblot Analyses
  - Quantitative Real-Time PCR Analysis
  - Serum ALT Assay
  - Histology
  - In Situ Hybridization (ISH)
  - Chromatin Immunoprecipitation (ChIP) Assays
  - Statistical Analysis

SUPPLEMENTAL INFORMATION

Supplemental Information includes seven figures and two tables and can be found with this article online at https://doi.org/10.1016/j.ccell.2018.05.003.

ACKNOWLEDGMENTS

Research was supported by the Superfund Basic Research Program (P42ES010337) to M.K. and E.S., NIH (R01-CA118165) grant to M.K. D.D was supported by the ALF Liver scholar award and a Young Investigator Award from the CureSearch Foundation; S.S. by the fellowship from CRI-Irvington and PCF Young Investigator Award; L.A. by the iCARE Fellowship, AIRC (Associazione Italiana per la ricerca sul cancro) co-founded by the European Union; J.Y.K. by the AACR-Bayer HCC post-doctoral fellowship; H.N. by the JSPS KAKENHI Grant Number 15K19313, Japanese Society of Gastroenterology, and Astelas Foundation for Research on Metabolic Disorders; and L.Y. by the National Natural Science Foundation of China (30500658,

Figure 7. STAT3 Controls CD44 Expression in Pericentral Hepatocytes

(A and B) WT males were DEN-challenged (100 mg/kg) and the *Cd44* mRNA was analyzed by ISH in their livers (A) or by qRT-PCR in isolated hepatocytes (B) ($n \geq 3$ mice/group; ND, not detected).

(C and D) ChIP assays probing STAT3 recruitment to the *Cd44* promoter in DihXY cells with or without serum starvation (C), and with or without IL-6 stimulation (30 min) after serum starvation (D).

(E and F) WT mice were treated with Veh or AZD1480 (30 mg/kg/day) starting 1 day prior to DEN injection (100 mg/kg). Isolated hepatocytes were IB-analyzed as indicated (E), whereas *Cd44* mRNA was quantitated by qRT-PCR (F) ($n \geq 3$ mice/group). All bar graphs in (B–F) represent the mean ± SEM.

(G) Human liver adenomas were grouped based on *IL6ST* mutation status (M = mutated, NM = Not mutated) and *CD44* mRNA expression was quantitated. Results are expressed as Tukey's boxplots where box indicates the first and third quartiles, bar indicates median, whiskers indicate 1.5 IQR, and data beyond the whiskers represent outliers.

(H) Schematic representation of the CD44-Mdm2-p53 circuit that controls HCC initiation. DEN-exposed pericentral hepatocytes undergo DNA damage and mutagenesis. Extensively damaged cells die and release DAMPs that activate macrophages to produce cytokines (IL-6) and growth factors, including EGFR ligands. Hepatocytes with moderate DNA damage mount a DNA damage response that leads to p53 activation and induction of $p21^{Waf1}$, Noxa, and Puma, which mediate cell-cycle arrest or apoptosis. p53 also leads to Mdm2 induction. In pericentral cells, growth factors and IL-6 lead to induction of CD44, which potentiates EGFR and Akt activation, resulting in Mdm2 phosphorylation and nuclear translocation. Nuclear Mdm2 inhibits p53 activation and accumulation. Termination of the p53 response allows carcinogen-exposed pericentral hepatocytes to survive, proliferate, and transmit potentially oncogenic mutations to their progeny. $^{*}p \leq 0.05$, $^{**}p \leq 0.01$, $^{***}p \leq 0.001$. See also Figure S7.

81370550 and 81570530). S.L. and K.M. were supported by intramural grants from the FLI. J.T. was supported by the Boehringer Ingelheim Stiftung. Generation of *Cd44-Floxed* mice was supported by DFG grant He-551 to Peter Herrlich. We are grateful to Dr. Zhao-Qi Wang for advice in ES cell targeting and Dr. Milen Kirilov for providing targeting vectors and advice in the targeting strategy. M.S. was supported by the European Research Council (ERC) Advanced Grant 694883 and Austrian Science Fund special research program SFB F3518-B20. J.Z.R. was supported by the Ligue Nationale contre le Cancer (Equipe Labellisée), Labex OncoImmunology (investissement d'avenir), Coup d'Elan de la Fondation Bettencourt-Shueller, the SIRIC CARPEM, and Fondation Mérieux. We thank Souradipta Ganguly for help with experiments.

AUTHOR CONTRIBUTIONS

D.D. and M.K. conceived and designed the project. M.K. supervised the project. D.D. performed most of the experiments and analyzed data. L.A., S.S., H.N., and J.Y.K. provided assistance in experiments and data analyses. L.Y. and E.S. helped with the experiments related to $Tak1^{\Delta Hep}$ mice. E.G. and M.S. helped with the experiments related to $Egfr^{\Delta Mx}$ mice by providing tissue specimens. J.T. provided the $Cd44^{F/F}$ mice and provided technical expertise related to $Cd44^{F/F}$ mice along with S.L. and K.M. M.A.V. made pathological diagnosis. S.C. and J.Z.R. performed human HCC data analyses. M.K. and D.D. wrote the manuscript with all authors providing feedback and advice.

DECLARATION OF INTERESTS

The authors declare no competing interests.

Received: August 3, 2017
Revised: February 28, 2018
Accepted: May 6, 2018
Published: June 11, 2018

REFERENCES

Aubrey, B.J., Strasser, A., and Kelly, G.L. (2016). Tumor-suppressor functions of the TP53 pathway. Cold Spring Harb. Perspect. Med. *6*, https://doi.org/10.1101/cshperspect.a026062.

Bahar Halpern, K., Shenhav, R., Matcovitch-Natan, O., Toth, B., Lemze, D., Golan, M., Massasa, E.E., Baydatch, S., Landen, S., Moor, A.E., et al. (2017). Single-cell spatial reconstruction reveals global division of labour in the mammalian liver. Nature *542*, 352–356.

Bergmann, J., Muller, M., Baumann, N., Reichert, M., Heneweer, C., Bolik, J., Lucke, K., Gruber, S., Carambia, A., Boretius, S., et al. (2017). IL-6 trans-signaling is essential for the development of hepatocellular carcinoma in mice. Hepatology *65*, 89–103.

Bettermann, K., Vucur, M., Haybaeck, J., Koppe, C., Janssen, J., Heymann, F., Weber, A., Weiskirchen, R., Liedtke, C., Gassler, N., et al. (2010). TAK1 suppresses a NEMO-dependent but NF-kappaB-independent pathway to liver cancer. Cancer Cell *17*, 481–496.

Bourguignon, L.Y. (2008). Hyaluronan-mediated CD44 activation of RhoGTPase signaling and cytoskeleton function promotes tumor progression. Semin. Cancer Biol. *18*, 251–259.

Brown, R.L., Reinke, L.M., Damerow, M.S., Perez, D., Chodosh, L.A., Yang, J., and Cheng, C. (2011). CD44 splice isoform switching in human and mouse epithelium is essential for epithelial-mesenchymal transition and breast cancer progression. J. Clin. Invest. *121*, 1064–1074.

Buckley, A.F., Burgart, L.J., Sahai, V., and Kakar, S. (2008). Epidermal growth factor receptor expression and gene copy number in conventional hepatocellular carcinoma. Am. J. Clin. Pathol. *129*, 245–251.

Budanov, A.V., and Karin, M. (2008). p53 target genes sestrin1 and sestrin2 connect genotoxic stress and mTOR signaling. Cell *134*, 451–460.

Canettieri, G., Di Marcotullio, L., Greco, A., Coni, S., Antonucci, L., Infante, P., Pietrosanti, L., De Smaele, E., Ferretti, E., Miele, E., et al. (2010). Histone deacetylase and Cullin3-REN(KCTD11) ubiquitin ligase interplay regulates Hedgehog signalling through Gli acetylation. Nat. Cell Biol. *12*, 132–142.

Cederbaum, A.I. (2012). Alcohol metabolism. Clin. Liver Dis. *16*, 667–685.

Chakrabarti, S.K., James, J.C., and Mirmira, R.G. (2002). Quantitative assessment of gene targeting in vitro and in vivo by the pancreatic transcription factor, Pdx1. Importance of chromatin structure in directing promoter binding. J. Biol. Chem. *277*, 13286–13293.

Dahl, J.A., and Collas, P. (2007). Q2ChIP, a quick and quantitative chromatin immunoprecipitation assay, unravels epigenetic dynamics of developmentally regulated genes in human carcinoma cells. Stem Cells *25*, 1037–1046.

El-Serag, H.B., and Rudolph, K.L. (2007). Hepatocellular carcinoma: epidemiology and molecular carcinogenesis. Gastroenterology *132*, 2557–2576.

Endo, K., and Terada, T. (2000). Protein expression of CD44 (standard and variant isoforms) in hepatocellular carcinoma: relationships with tumor grade, clinicopathologic parameters, p53 expression, and patient survival. J. Hepatol. *32*, 78–84.

Fitzgerald, K.A., Bowie, A.G., Skeffington, B.S., and O'Neill, L.A. (2000). Ras, protein kinase C zeta, and I kappa B kinases 1 and 2 are downstream effectors of CD44 during the activation of NF-kappa B by hyaluronic acid fragments in T-24 carcinoma cells. J. Immunol. *164*, 2053–2063.

Flanagan, B.F., Dalchau, R., Allen, A.K., Daar, A.S., and Fabre, J.W. (1989). Chemical composition and tissue distribution of the human CDw44 glycoprotein. Immunology *67*, 167–175.

Font-Burgada, J., Shalapour, S., Ramaswamy, S., Hsueh, B., Rossell, D., Umemura, A., Taniguchi, K., Nakagawa, H., Valasek, M.A., Ye, L., et al. (2015). Hybrid periportal hepatocytes regenerate the injured liver without giving rise to cancer. Cell *162*, 766–779.

Fridman, J.S., and Lowe, S.W. (2003). Control of apoptosis by p53. Oncogene *22*, 9030–9040.

Fuchs, B.C., Hoshida, Y., Fujii, T., Wei, L., Yamada, S., Lauwers, G.Y., McGinn, C.M., DePeralta, D.K., Chen, X., Kuroda, T., et al. (2014). Epidermal growth factor receptor inhibition attenuates liver fibrosis and development of hepatocellular carcinoma. Hepatology *59*, 1577–1590.

Gartel, A.L., and Tyner, A.L. (2002). The role of the cyclin-dependent kinase inhibitor p21 in apoptosis. Mol. Cancer Ther. *1*, 639–649.

Godar, S., Ince, T.A., Bell, G.W., Feldser, D., Donaher, J.L., Bergh, J., Liu, A., Miu, K., Watnick, R.S., Reinhardt, F., et al. (2008). Growth-inhibitory and tumor-suppressive functions of p53 depend on its repression of CD44 expression. Cell *134*, 62–73.

Gregorieff, A., Pinto, D., Begthel, H., Destree, O., Kielman, M., and Clevers, H. (2005). Expression pattern of Wnt signaling components in the adult intestine. Gastroenterology *129*, 626–638.

He, G., Dhar, D., Nakagawa, H., Font-Burgada, J., Ogata, H., Jiang, Y., Shalapour, S., Seki, E., Yost, S.E., Jepsen, K., et al. (2013). Identification of liver cancer progenitors whose malignant progression depends on autocrine IL-6 signaling. Cell *155*, 384–396.

He, G., Yu, G.Y., Temkin, V., Ogata, H., Kuntzen, C., Sakurai, T., Sieghart, W., Peck-Radosavljevic, M., Leffert, H.L., and Karin, M. (2010). Hepatocyte IKKbeta/NF-kappaB inhibits tumor promotion and progression by preventing oxidative stress-driven STAT3 activation. Cancer Cell *17*, 286–297.

Hedvat, M., Huszar, D., Herrmann, A., Gozgit, J.M., Schroeder, A., Sheehy, A., Buettner, R., Proia, D., Kowolik, C.M., Xin, H., et al. (2009). The JAK2 inhibitor AZD1480 potently blocks Stat3 signaling and oncogenesis in solid tumors. Cancer Cell *16*, 487–497.

Hijmans, B.S., Grefhorst, A., Oosterveer, M.H., and Groen, A.K. (2014). Zonation of glucose and fatty acid metabolism in the liver: mechanism and metabolic consequences. Biochimie *96*, 121–129.

Hoeijmakers, J.H. (2009). DNA damage, aging, and cancer. N. Engl. J. Med. *361*, 1475–1485.

Hong, H., Takahashi, K., Ichisaka, T., Aoi, T., Kanagawa, O., Nakagawa, M., Okita, K., and Yamanaka, S. (2009). Suppression of induced pluripotent stem cell generation by the p53-p21 pathway. Nature *460*, 1132–1135.

Huh, C.G., Factor, V.M., Sanchez, A., Uchida, K., Conner, E.A., and Thorgeirsson, S.S. (2004). Hepatocyte growth factor/c-met signaling pathway is required for efficient liver regeneration and repair. Proc. Natl. Acad. Sci. USA *101*, 4477–4482.

Inokuchi, S., Aoyama, T., Miura, K., Osterreicher, C.H., Kodama, Y., Miyai, K., Akira, S., Brenner, D.A., and Seki, E. (2010). Disruption of TAK1 in hepatocytes causes hepatic injury, inflammation, fibrosis, and carcinogenesis. Proc. Natl. Acad. Sci. USA *107*, 844–849.

Inokuchi-Shimizu, S., Park, E.J., Roh, Y.S., Yang, L., Zhang, B., Song, J., Liang, S., Pimienta, M., Taniguchi, K., Wu, X., et al. (2014). TAK1-mediated autophagy and fatty acid oxidation prevent hepatosteatosis and tumorigenesis. J. Clin. Invest. *124*, 3566–3578.

Jonkers, J., Meuwissen, R., van der Gulden, H., Peterse, H., van der Valk, M., and Berns, A. (2001). Synergistic tumor suppressor activity of BRCA2 and p53 in a conditional mouse model for breast cancer. Nat. Genet. *29*, 418–425.

Kang, J.S., Wanibuchi, H., Morimura, K., Gonzalez, F.J., and Fukushima, S. (2007). Role of CYP2E1 in diethylnitrosamine-induced hepatocarcinogenesis in vivo. Cancer Res. *67*, 11141–11146.

Kinjyo, I., Inoue, H., Hamano, S., Fukuyama, S., Yoshimura, T., Koga, K., Takaki, H., Himeno, K., Takaesu, G., Kobayashi, T., et al. (2006). Loss of SOCS3 in T helper cells resulted in reduced immune responses and hyperproduction of interleukin 10 and transforming growth factor-beta 1. J. Exp. Med. *203*, 1021–1031.

Kopp, J.L., von Figura, G., Mayes, E., Liu, F.F., Dubois, C.L., Morris, J.P.T., Pan, F.C., Akiyama, H., Wright, C.V., Jensen, K., et al. (2012). Identification of Sox9-dependent acinar-to-ductal reprogramming as the principal mechanism for initiation of pancreatic ductal adenocarcinoma. Cancer Cell *22*, 737–750.

Lanaya, H., Natarajan, A., Komposch, K., Li, L., Amberg, N., Chen, L., Wculek, S.K., Hammer, M., Zenz, R., Peck-Radosavljevic, M., et al. (2014). EGFR has a tumour-promoting role in liver macrophages during hepatocellular carcinoma formation. Nat. Cell Biol. *16*, 972–981, 971–977.

Lane, D., and Levine, A. (2010). p53 research: the past thirty years and the next thirty years. Cold Spring Harb. Perspect. Biol. *2*, a000893.

Lee, J.L., Wang, M.J., and Chen, J.Y. (2009). Acetylation and activation of STAT3 mediated by nuclear translocation of CD44. J. Cell Biol. *185*, 949–957.

Maeda, S., Kamata, H., Luo, J.L., Leffert, H., and Karin, M. (2005). IKKbeta couples hepatocyte death to cytokine-driven compensatory proliferation that promotes chemical hepatocarcinogenesis. Cell *121*, 977–990.

Mas, V.R., Maluf, D.G., Archer, K.J., Yanek, K., Kong, X., Kulik, L., Freise, C.E., Olthoff, K.M., Ghobrial, R.M., McIver, P., et al. (2009). Genes involved in viral carcinogenesis and tumor initiation in hepatitis C virus-induced hepatocellular carcinoma. Mol. Med. *15*, 85–94.

Mayo, L.D., and Donner, D.B. (2001). A phosphatidylinositol 3-kinase/Akt pathway promotes translocation of Mdm2 from the cytoplasm to the nucleus. Proc. Natl. Acad. Sci. USA *98*, 11598–11603.

Michael, D., and Oren, M. (2002). The p53 and Mdm2 families in cancer. Curr. Opin. Genet. Dev. *12*, 53–59.

Natarajan, A., Wagner, B., and Sibilia, M. (2007). The EGF receptor is required for efficient liver regeneration. Proc. Natl. Acad. Sci. USA *104*, 17081–17086.

Naugler, W.E., Sakurai, T., Kim, S., Maeda, S., Kim, K., Elsharkawy, A.M., and Karin, M. (2007). Gender disparity in liver cancer due to sex differences in MyD88-dependent IL-6 production. Science *317*, 121–124.

Nault, J.C., De Reynies, A., Villanueva, A., Calderaro, J., Rebouissou, S., Couchy, G., Decaens, T., Franco, D., Imbeaud, S., Rousseau, F., et al. (2013). A hepatocellular carcinoma 5-gene score associated with survival of patients after liver resection. Gastroenterology *145*, 176–187.

Orian-Rousseau, V., Chen, L., Sleeman, J.P., Herrlich, P., and Ponta, H. (2002). CD44 is required for two consecutive steps in HGF/c-Met signaling. Genes Dev. *16*, 3074–3086.

Park, E.J., Lee, J.H., Yu, G.Y., He, G., Ali, S.R., Holzer, R.G., Osterreicher, C.H., Takahashi, H., and Karin, M. (2010). Dietary and genetic obesity promote liver inflammation and tumorigenesis by enhancing IL-6 and TNF expression. Cell *140*, 197–208.

Pilati, C., Letouze, E., Nault, J.C., Imbeaud, S., Boulai, A., Calderaro, J., Poussin, K., Franconi, A., Couchy, G., Morcrette, G., et al. (2014). Genomic profiling of hepatocellular adenomas reveals recurrent FRK-activating mutations and the mechanisms of malignant transformation. Cancer Cell *25*, 428–441.

Ponta, H., Sherman, L., and Herrlich, P.A. (2003). CD44: from adhesion molecules to signalling regulators. Nat. Rev. Mol. Cell Biol. *4*, 33–45.

Protin, U., Schweighoffer, T., Jochum, W., and Hilberg, F. (1999). CD44-deficient mice develop normally with changes in subpopulations and recirculation of lymphocyte subsets. J. Immunol. *163*, 4917–4923.

Sakurai, T., He, G., Matsuzawa, A., Yu, G.Y., Maeda, S., Hardiman, G., and Karin, M. (2008). Hepatocyte necrosis induced by oxidative stress and IL-1 alpha release mediate carcinogen-induced compensatory proliferation and liver tumorigenesis. Cancer Cell *14*, 156–165.

Shalapour, S., Lin, X.J., Bastian, I.N., Brain, J., Burt, A.D., Aksenov, A.A., Vrbanac, A.F., Li, W., Perkins, A., Matsutani, T., et al. (2017). Inflammation-induced IgA+ cells dismantle anti-liver cancer immunity. Nature *551*, 340–345.

Sharma, A., Singh, K., and Almasan, A. (2012). Histone H2AX phosphorylation: a marker for DNA damage. Methods Mol. Biol. *920*, 613–626.

Shi, D., and Gu, W. (2012). Dual roles of MDM2 in the regulation of p53: ubiquitination dependent and ubiquitination independent mechanisms of MDM2 repression of p53 activity. Genes Cancer *3*, 240–248.

Soltoff, S.P., Carraway, K.L., 3rd, Prigent, S.A., Gullick, W.G., and Cantley, L.C. (1994). ErbB3 is involved in activation of phosphatidylinositol 3-kinase by epidermal growth factor. Mol. Cell. Biol. *14*, 3550–3558.

Spencer, S.L., Cappell, S.D., Tsai, F.C., Overton, K.W., Wang, C.L., and Meyer, T. (2013). The proliferation-quiescence decision is controlled by a bifurcation in CDK2 activity at mitotic exit. Cell *155*, 369–383.

Vassilev, L.T., Vu, B.T., Graves, B., Carvajal, D., Podlaski, F., Filipovic, Z., Kong, N., Kammlott, U., Lukacs, C., Klein, C., et al. (2004). In vivo activation of the p53 pathway by small-molecule antagonists of MDM2. Science *303*, 844–848.

Vousden, K.H., and Lu, X. (2002). Live or let die: the cell's response to p53. Nat. Rev. Cancer *2*, 594–604.

Vries, R.G., Huch, M., and Clevers, H. (2010). Stem cells and cancer of the stomach and intestine. Mol. Oncol. *4*, 373–384.

Weglarz, T.C., Degen, J.L., and Sandgren, E.P. (2000). Hepatocyte transplantation into diseased mouse liver. Kinetics of parenchymal repopulation and identification of the proliferative capacity of tetraploid and octaploid hepatocytes. Am. J. Pathol. *157*, 1963–1974.

Weinberg, R.A. (2013). The Biology of Cancer, Second Edition (Garland Science).

Wielenga, V.J., Smits, R., Korinek, V., Smit, L., Kielman, M., Fodde, R., Clevers, H., and Pals, S.T. (1999). Expression of CD44 in Apc and Tcf mutant mice implies regulation by the WNT pathway. Am. J. Pathol. *154*, 515–523.

Wu, H., Wade, M., Krall, L., Grisham, J., Xiong, Y., and Van Dyke, T. (1996). Targeted in vivo expression of the cyclin-dependent kinase inhibitor p21 halts hepatocyte cell-cycle progression, postnatal liver development and regeneration. Genes Dev. *10*, 245–260.

Yamashita, T., and Wang, X.W. (2013). Cancer stem cells in the development of liver cancer. J. Clin. Invest. *123*, 1911–1918.

Zhou, B.P., Liao, Y., Xia, W., Zou, Y., Spohn, B., and Hung, M.C. (2001). HER-2/neu induces p53 ubiquitination via Akt-mediated MDM2 phosphorylation. Nat. Cell Biol. *3*, 973–982.

Zoller, M. (2011). CD44: can a cancer-initiating cell profit from an abundantly expressed molecule? Nat. Rev. Cancer *11*, 254–267.

STAR★METHODS

KEY RESOURCES TABLE

REAGENT or RESOURCE	SOURCE	IDENTIFIER
Antibodies		
anti-CD44pan (DF1485)	Santa Cruz Biotechnology	Cat# SC-7297; RRID: AB_627065
anti-CD44pan (IM7)	ABDSerotec (Biorad)	Cat# MCA4703; RRID: AB_2076194
anti-CD44v6	ABD Serotec (Biorad)	Cat# MCA1967; RRID: AB_323213
anti-AFP	R&D Systems	Cat# AF5369; RRID: AB_2258018
anti-Ki67	Genetex	Cat# GTX16667; RRID: AB_422351
anti-F4/80 (Clone: A3-1)	Caltag/Thermo Fisher	Cat# MA1-91124; RRID: AB_2277854
anti-Clvd. Caspase 3	Cell Signaling Technologies	Cat# CS9661; RRID: AB_2341188
anti-p-p53(Ser15)	Cell Signaling Technologies	Cat# CS9284; RRID: AB_331464
anti-p53	Leica Biosystems	Cat# NCL-p53-CM5p; RRID: AB_563933
anti-MDM2 (2A10)	Millipore	Cat# OP115; RRID: AB_213269
anti-p-MDM2 (Ser166)	Cell Signaling Technologies	Cat# CS3521; RRID: AB_2143550
anti-p-AKT (Ser473) (IHC)	Cell Signaling Technologies	Cat# CS3787; RRID: AB_331170
anti-p-AKT (Ser473)	Cell Signaling Technologies	Cat# CS9271; RRID: AB_329825
anti-p-EGFR (Y1068)	Cell Signaling Technologies	Cat# CS3777; RRID: AB_2096270
anti-tEGFR	Cell Signaling Technologies	Cat# CS4267; RRID: AB_2246311
anti-p-H2AX (Ser139)	Cell Signaling Technologies	Cat# CS9718; RRID: AB_2118009
anti-Cyp2E1	Millipore	Cat# AB1252; RRID: AB_11212002
anti-Noxa	Santa Cruz	Cat# SC56169; RRID: AB_784877
anti-Puma	Santa Cruz	Cat# SC377015; RRID: AB_2714161
anti-p21	Millipore	Cat# MAB88058; RRID: AB_2291542
anti-p21 (IHC)	Abcam	Cat# ab188224
anti-Tubulin	Sigma	Cat# T5168; RRID: AB_477579
anti-p-STAT3 (Y705)	Cell Signaling Technologies	Cat# CS9131; RRID: AB_331586
anti-tSTAT3	Cell Signaling Technologies	Cat# CS12640; RRID: AB_2629499
anti-tSTAT3 (C-20) (ChIP)	Santa Cruz Biotechnology	Cat# sc-482; RRID: AB_632440
rabbit IgG (ChIP)	Santa Cruz Biotechnology	Cat# sc-2027; RRID: AB_737197
anti-digoxigenin-AP	Roche	Cat# 11093274910; RRID: AB_514497
Biological Samples		
Human HCC tissue array	US Biomax, Inc.	Cat# LV1501
Fresh-frozen human HCC and normal tissue samples	Jessica Zucman–Rossi (INSERM) and Oncomine (Mas et al., 2009; Nault et al., 2013)	N/A
Fresh-frozen human HCA tissue samples	Jessica Zucman–Rossi (INSERM) (Pilati et al., 2014)	N/A
Chemicals, Peptides, and Recombinant Proteins		
N-Nitrosodiethylamine (DEN)	Sigma	Cat# N0258-1G
Recombinant Murine IL-6	Peprotech	Cat# 216-16
(±)-Nutlin-3	Cayman Chemicals	Cat# 10004372
MK2206	MedChem Express	Cat# HY-10358
Gefitinib (ZD1839)	MedChem Express	Cat# HY-50895
AZD1480	AstraZeneca (Hedvat et al., 2009)	N/A
Cisplatin	APP Pharmaceuticals	Cat# 100351
Collagen I, Rat Tail	Corning	Cat# 354236
Waymouth's medium	Gibco	Cat# 11220035
Protein A dynabeads	Invitrogen/ Thermo Scientific	Cat# 10001D

(*Continued on next page*)

Continued

REAGENT or RESOURCE	SOURCE	IDENTIFIER
Protein A Agarose beads	Upstate/ Millipore	Cat# 16-125
RNase A	Thermo Scientific	Cat# EN0531
Proteinase K Solution, ChIP grade	Thermo Scientific	Cat# 26160
Liberase-TM	Roche	Cat# 5401127001
Blocking Reagent	Roche	Cat# 11096176001
Critical Commercial Assays		
ALT (GPT) reagent	Thermo Scientific	Cat# TR71121
In Situ Cell Death Detection Kit, TMR red (TUNEL assay)	Roche	Cat# 12156792910
ImmPRESS™ HRP Anti-Rabbit IgG (Peroxidase) Polymer Detection Kit	Vector Laboratories	Cat# MP-7401
ImmPRESS™ Excel Amplified HRP Polymer Staining Kit (Anti-Rabbit IgG)	Vector Laboratories	Cat# MP-7601
VECTOR Red Alkaline Phosphatase (Red AP) Substrate Kit	Vector Laboratories	Cat# SK-5100
Mouse on Mouse (M.O.M.™) ImmPRESS™ HRP (Peroxidase) Polymer Kit	Vector Laboratories	Cat# MP-2400
ImmPACT DAB Peroxidase (HRP) Substrate	Vector Laboratories	Cat# SK-4105
NE-PER™ Nuclear and Cytoplasmic Extraction Reagents	Thermo Scientific	Cat# 78833
DIG RNA Labeling Kit	Roche	Cat# 11175025910
In Situ Hybridization m*Mdm2* probe	ACDbio/Biotechne	Cat# 447641
RNAscope 2.5 HD Assay kit- BROWN	ACDbio/Biotechne	Cat# 322310
Super Script VILO cDNA synthesis kit	Thermo Scientific	Cat# 11754050
RNeasy Mini Kit	Qiagen	Cat# 74104
SsoAdvance SYBR Green Supermix	Biorad	Cat# 1725275
BCIP/NBT Color Development Substrate	Promega	Cat# S3771
Experimental Models: Cell Lines		
Dih10	The Karin Laboratory (He et al., 2013)	N/A
DihXY	The Karin Laboratory (He et al., 2010; Shalapour et al., 2017)	N/A
Experimental Models: Organisms/Strains		
Mouse: C57BL/6	Charles River Laboratories	Strain Code: 027
Mouse: *Cd44*$^{-/-}$	The Jackson Laboratory	Stock# 005085
Mouse: *p53*$^{F/F}$	Anton Berns (Budanov and Karin, 2008) (Jonkers et al., 2001)	N/A
Mouse: *p21*$^{-/-}$	The Jackson Laboratory	Stock# 016565
Mouse: *Cd44*$^{F/F}$	This paper, Peter Herrlich (FLI, Germany)	N/A
Mouse: *Albumin-Cre*	The Jackson Laboratory	Stock# 003574
Mouse: *EGFR*$^{F/F}$	Maria Sibilia (Lanaya et al., 2014)	N/A
Mouse: *Mx1Cre*	Maria Sibilia (Lanaya et al., 2014)	N/A
Mouse: *MUP-uPA*	Eric P. Sandgren (Weglarz et al., 2000)	N/A
Mouse: *Tak1*$^{\Delta Hep}$	Ekihiro Seki (Inokuchi et al., 2010)	N/A
Oligonucleotides		
ChIP Primer, m*Cd44* promoter, forward: ATGGGCTGGATTTCCACATA	This paper	N/A
ChIP Primer, m*Cd44* promoter, reverse: CCTTTCTCCTCCCAGTCTCC	This paper	N/A

(*Continued on next page*)

Continued		
REAGENT or RESOURCE	SOURCE	IDENTIFIER
ChIP negative control Primer, m*Cd44* promoter, forward: GACTTCTCCCCCTTTTCTGC	This paper	N/A
ChIP negative control Primer, m*Cd44* promoter, reverse: GCACCTAACCTTCCCTGGTT	This paper	N/A
ChIP Primer, mc-*Fos* promoter, forward: TCTGCCTTTCCCGCCTCCCC	(Kinjyo et al., 2006)	N/A
ChIP Primer, mc-*Fos* promoter, reverse: GGCCGTGGAAACCTGCTGAC	(Kinjyo et al., 2006)	N/A
ChIP Primer, m*Gapdh* promoter, forward: TTGAGCTAGGACTGGATAAGCAGGG	This paper	N/A
ChIP Primer, m*Gapdh* promoter, reverse: GTCCGTATTTATAGGAACCCGGATGGTG	This paper	N/A
Primers for analysis of gene-expression changes, see Table S2	The Karin Laboratory	N/A
Recombinant DNA		
mCD44 cDNA	Open biosystems/ Dharmacon	Clone ID# 4910789 Cat # MMM1013-202766790
Software and Algorithms		
GraphPad Prism 7.0 software	GraphPad Software, Inc.	www.graphpad.com/scientific-software/prism/
R software version 3.3.2	R Foundation for Statistical Computing, Vienna, Austria	http://www.r-project.org
Image Studio Lite Software	LI-COR	www.licor.com
Adobe Illustrator CS6	Adobe	www.adobe.com

CONTACT FOR REAGENT AND RESOURCE SHARING

Further information and requests for resources and reagents should be directed to and will be fulfilled according to institutional rules by the Lead Contact, Michael Karin (karinoffice@ucsd.edu).

EXPERIMENTAL MODEL AND SUBJECT DETAILS

Mice

Experiments were performed in accordance to the University of California San Diego (UCSD) Institutional Animal Care and Use Committee (IACUC) and NIH guidelines. Dr. Karin's Animal Protocol S00218 was approved by the UCSD IACUC. Experiments done in the Medical University of Vienna were approved by the Animal Experimental Ethics Committee of the Medical University of Vienna and the Austrian Federal Ministry of Science and Research (Animal license numbers: BMWFW-66.009/0200-WF/II/3b/2014; and BMWFW-66.009/0199-WF/II/3b/2014).

C57BL/6 mice were from Charles River Laboratories (Strain code# 027). *Cd44*$^{-/-}$ (Stock# 005085) and *Cdkn1*$^{-/-}$ (Stock# 016565) mice were from the Jackson Laboratories. *Tak1*$^{\Delta Hep}$ (Inokuchi et al., 2010), *Trp53*$^{\Delta Hep}$ (Budanov and Karin, 2008), *MUP-uPA* (He et al., 2013; Weglarz et al., 2000), and *Egfr*$^{F/F}$ (Lanaya et al., 2014) mice were described.

To induce HCC, 15-day-old males were i.p. injected with 25 mg/kg DEN (Sigma N0258) and livers were analyzed 9 months later. For acute DEN studies, 15-day-old male mice were i.p. injected with 25 mg/kg DEN and 8-12-week-old male mice were i.p. injected with 100 mg/kg DEN and liver and serum were analyzed at indicated time points. Only male mice were used and the number of mice per experiment and their age are indicated in the figure legends.

Generation of Cd44^{flox} *Mice*

Cd44$^{F/F}$ mice (in which constant exon 3 is floxed, after a *flrt neo*-cassette 3' of exon 3 had been removed upon gene targeting in ES cells) originally generated in the 129 Sv background were backcrossed to C57BL/6J mice for at least nine generations (FLI, Germany). A 1583 bp PCR fragment containing constant exon 3 of the murine *Cd44* gene was subcloned into the pLoxPFrt tkneoFrt targeting vector (courtsey of Milen Kirilov), 3' to a *LoxP Frt TK Neo Frt* cassette. The *TK-Neo* cassette was flanked by a 5' 1419 bp homology arm and a 3' 1583 bp fragment followed by the second LoxP site, at the 5' end of the 4912 bp 3' homology arm. 1583 bp, 1419 bp, and 4912 bp PCR fragments were amplified from genomic DNA of 129Sv/Ev mice and a 129Sv/Ev BAC clone and cloned into a pCR™Blunt II-TOPO® vector (ThermoFisher Scientific). A DTA cassette was subcloned from a pDTA vector (courtsey of Milen Kirilov) into the targeting vector upstream of the 5' homolgy arm and served for negative selection of successful homologous recombination

events in ES cells. The *Tk-Neo* cassette had been removed upon gene targeting in ES cells. $Cd44^{\Delta Hep}$ mice were generated by crossing $Cd44^{F/F}$ and *Alb-Cre* mice.

Cell Lines

Mouse HCC cell lines Dih10 (female) and DihXY (male) were established from DEN induced HCC tumors (He et al., 2010, 2013; Shalapour et al., 2017). Both cell lines were cultured in Dulbecco's Modified Eagle Medium (DMEM) with 20% FBS, 0.01 g/L Insulin, 0.01 g/L Hydrocortisone hemisuccinate, 1% Penn-Strep, 1% L-Glutamine, 1 mM Phenobarbital, and 20 μg/L Epidermal Growth Factor (EGF).

Primary Cells

Primary hepatocytes and HcPC were isolated from male mouse (with or without DEN treatment). Isolation procedure and culturing conditions are described in the detailed STAR Methods section.

Human Samples and Study Approval

The study was approved by Institutional Review Board committees (CCPRB Paris Saint Louis, 1997, 2004 and 2010). All patients gave their written informed consent in accordance with French legislation. A total of 250 fresh-frozen tissue samples of human HCC, including 5 HCC resulting from malignant transformation of hepatocellular adenomas (HCC on HCA), and 5 normal liver tissue samples were included in this study. Patients and tumor features were already described in a previously published study (Nault et al., 2013) (Table S1). Briefly, among the 250 HCC patients, 80.8% were male, with a median age of 65 years old and associated with various risk factors (alcohol intake, HCV, HBV, hemochromatosis, metabolic syndrome and with no known etiology). Most of the HCC samples were "moderately differentiated" according to WHO classification and Edmondson-Steiner grading system. The proportions of mutations on the main driver genes in these HCC samples are in line with what was previously published (*TERT* promoter mutations: 63.8%; *CTNNB1* mutations: 40.5%; *TP53* mutations: 21.6%).

CD44 mRNA levels were also assessed in a large cohort of 222 HCA tissue samples, already included in a previously published study (Pilati et al., 2014). Among the 222 HCA samples, 62 (27.9%) were inflammatory adenomas caused by *IL6ST* somatic mutation activating gp130.

The data for U.S. HCC cohort was obtained from the public database www.ncbi.nlm.nih.gov/geo/query/acc.cgi?acc=GSE14323 (Mas et al., 2009). Affymetrix Human Genome U133A 2.0 array was used to determine *Cd44* expression levels (probe 204490_s_at).

IHC Analysis of Human HCC

HCC tissue array was purchased from US Biomax that contained 60 paired human HCC and nontumor tissues. Usage of the tissue array is IRB exempt under the UCSD Human Research Protections Program Standard Operating Policies and Procedures (SOPPs). When the number of CD44 or pMDM2-positive cells was $\geq$ 5%, the sample was defined as positive.

mRNA Analysis in Human Tumors

CD44 gene expression levels were assessed by quantitative RT-PCR using Fluidigm 96.96 Dynamic Arrays and a specific TaqMan predesigned assay (Hs01075861_m1; Life Technologies, Carlsbad, CA). Data were calibrated with the RNA ribosomal 18S and changes in mRNA expression levels were determined using a comparative CT method.

METHOD DETAILS

Cell Culture and *In Vitro* Treatments

Dih mouse HCC cell lines were cultured and mentioned above and were treated with the following compounds as indicated: pan-AKT inhibitor MK2206 (MedChem Express# HY-10358); Nutlin-3 (Cayman chemicals# 10004372); Cisplatin (APP Pharmaceuticals #100351). For cell culture treatments over 24 hr in duration, the media containing the compounds were replaced every day.

Primary hepatocytes were isolated from 8-12-week-old male mice (untreated or DEN treated) by perfusing the liver with Liberase-TM (Roche# 05401127001) through inferior vena cava (IVC). Hepatocytes were purified by low speed (50 g) differential centrifugation and repeated washes (3x) with PBS. Cells were snap frozen in liquid nitrogen for RNA and protein analyses at later time. For IL-6 stimulation, cells were cultured overnight in Waymouth's medium (Gibco# 11220035) in type-1 collagen coated plates (Rat tail, Corning 354236) and stimulated with 20 ng/ml IL-6 (PeproTech# 216-16).

HcPC from tumor bound mouse livers were isolated by Liberase-TM perfusion as mentioned above and subsequent filtration of the isolated cells through 70 and 40 μm sieves (He et al., 2013). The aggregated cell population (HcPC) retained on top of the filter are collected in Ca/Mg-free PBS. To disperse the aggregates into single cells, they were subjected to gentle pipetting in PBS on ice. Single-cell suspensions of aggregated hepatocytes were transplanted via an intrasplenic (i.s.) injection into 21-day-old male *MUP-uPA* mice.

In Vivo Treatments

Jak1/2 inhibitor (AZD1480 AstraZeneca) (Hedvat et al., 2009) was dissolved in 0.5% HPMC/ 0.1% TWEEN 80 (Veh) and was administered at the dose of 30 mg/kg by oral gavage, once daily to 8-12-week old mice. AZD1480 dosing started 24 hr prior to DEN injection (100 mg/kg in PBS). EGFR inhibitor Gefitinib (ZD1839) and pan-AKT inhibitor (MK2206) at the dose of 100 mg/kg or Veh (corn oil + 5% DMSO) was administered by oral gavage, once daily to 8-12-week old mice starting one day prior to DEN injection (100 mg/kg).

Nuclear-Cytoplasmic Extraction and Immunoblot Analyses

NE-Per Nuclear and cytoplasmic extraction kit (Thermo Scientific# 78833) was used for nuclear and cytosolic fractionation of cells and liver tissues. Livers were homogenized by dounce homogenizer (Thomas Scientific, NJ) with 30 strokes and cytosolic and nuclear factions were separated as per the manufacturer's protocol. Whole cell or whole tissue lysates were made in RIPA buffer with protease and phosphatase inhibitors. IB analysis was performed on cell or tissue lysates that were separated by SDS-PAGE and transferred to PVDF membranes. Antibody details are provided in the Key Resources Table.

Quantitative Real-Time PCR Analysis

RNA samples were prepared using RNeasy kit (Qiagen# 74104). RNA was reverse transcribed using a Super Script VILO cDNA synthesis kit (Thermo Scientific# 11754050) and qPCR was performed using SYBR green (Biorad# 1725275) based real-time PCR on a Biorad CFX96 machine. Relative mRNA expression was calculated form the comparative threshold cycle (Ct) values relative to the ribosomal protein S23 mRNA. PCR primers were designed using online primer tools Primer3 or Primer Depot and purchased from Integrated DNA Technologies. Primer sequences are provided in Table S2.

Serum ALT Assay

Serum ALT levels were measured using Infinity ALT (GPT) reagent (Thermo scientific# TR71121) according to the supplied protocol.

Histology

Mouse liver samples were fixed with 10% neutral buffered formalin and paraffin embedded. 5μm thick sections were stained with hematoxylin and eosin (H&E) and processed for IHC. Vector Labs M.O.M kit (MP2400) was used for blocking endogenous mouse IgG when detecting mouse proteins using mouse primary antibodies. Vector Labs ImmPRESS™ Excel Amplified HRP Polymer Staining Kit (MP7601) was used for IHCs that required signal amplification. Antibody details are provided in the Key Resources Table.

TUNEL staining was performed using an *in-situ* cell death detection kit (Roche# 12156792910). Images were captured on an upright light/fluorescent microscope (Zeiss) equipped with an AxioCam camera.

In Situ Hybridization (ISH)

CD44 cDNA (Open biosystems clone ID# 4910789), linearized with SalI restriction digestion, was used to prepare digoxigenin (DIG)-labeled RNA probes by *in vitro* transcription reaction using T7 RNA polymerase (Roche kit: 11175025910) following manufacturer's protocol. The DIG-labeled cRNA probes were purified with Qiagen RNeasy kit and were used for ISH on formalin-fixed paraffin-embedded liver sections as described (Gregorieff et al., 2005). Briefly, formalin-fixed paraffin embedded (FFPE) liver sections were dewaxed and rehydrated using xylene and decreasing concentrations of ethanol (100%-96%-70%-50%-25% ethanol, 5 min each) and rinsed with DEPC-treated water. Sections were treated with 0.2 N HCl for 15 min and incubated with 30 μg/ml proteinase K in PBS at 37°C for 20 min; rinsed in 0.2% glycine/PBS solution and then twice in PBS. Sections were incubated in acetic anhydride solution (0.25% acetic anhydride in 0.1 M Triethanolamine pH 8.0) for 5 min and washed in PBS and 5X SSC. Sections were then pre-hybridized with 5X SSC/50% formamide in a 65°C oven for at least 1 hour and then with the DIG-labeled probe (500 ng/ml) diluted in hybridization solution [50% Formamide, 5X SSC pH 4.5, 2% Blocking reagent (Roche: 11096176001), 0.05% CHAPS, 5 mM EDTA, 50 μg/ml heparin, 1 μg/ml yeast RNA]. Slides were incubated in an oven at 62-70°C for 16-72 hours. After incubation, slides were washed 3x for 20 min at 60-65°C in 50% formamide/2X SSC pH 4.5 and 5X in Tris-NaCl buffer. Finally, DIG-labeled probes were immunodetected using an anti-digoxigenin AP-conjugated antibody (Roche: 11093274910) and developed using NBT/BCIP substrate kit (Promega: S3771).

For MDM2 ISH, MDM2 probes and detection kit from RNAscope (ACD Bio Cat# 447641 and Cat# 322310 respectively) were used and mouse liver sections were stained according to the manufacturers protocol.

Chromatin Immunoprecipitation (ChIP) Assays

Cells were crosslinked 10 min with 1% formaldehyde and the reaction was stopped with 0.125 M Glycine for 5 min. Cells were washed, harvested with PBS supplemented with protease inhibitors, and the cytoplasmatic membranes lysed with lysis buffer (5 mM PIPES, 85 mM KCl, 0.5% NP40). After centrifugation, nuclei were lysed 10 min in ice with sonication buffer (1% SDS, 10 mM EDTA, 50 mM TRIS pH 8 supplemented with protease inhibitors) and sonicated to obtain chromatin fragments of about 400-600 nucleotides. The lysates were precleared for 1 hr at 4°C with 30 μl of protein A agarose (Upstate/Millipore# 16-125), then supernatant was collected, and 10% of each sample was saved for input. Chromatin diluted with 9 volumes of dilution buffer (0.01% SDS, 1.2 mM EDTA, 16.7 mM Tris HCl pH 8, 1.1% Triton X-100, 167 mM NaCl, protease inhibitors) was incubated overnight with 20μl of Protein A dynabeads (Invitrogen# 10001D) coated with rabbit anti-STAT3 (2 μg), (Santa Cruz# sc-482), or rabbit IgG (Santa Cruz# sc-2027) as control as described (Dahl and Collas, 2007). The day after the immunocomplexes were washed 5 times with Buffer A (0.1% SDS, 2 mM EDTA, 20 mM Tris HCl pH 8, 1% Triton X-100, 150 mM NaCl), 4 times with buffer B (0.1% SDS, 2 mM EDTA, 20 mM Tris HCl pH 8, 1% Triton X-100, 500 mM NaCl), and once with Buffer T.E. (10 mM Tris HCl pH 8, 1 mM EDTA). After the final wash, the immunocomplexes, were eluted twice, with 250 μl elution buffer (1% SDS, 100 mM NaHCO3) 15 min in rotation at RT and, upon addition of 200 mM NaCl, the crosslinking reversed with an overnight incubation at 65°C. After de-crosslinking, the samples were digested with proteinase K (Thermo Scientific# 26160) and RNase A (Thermo Scientific# EN0531), 2 hr at 42°C, and the DNA purified and precipitated. Eluted DNA were analyzed by real-time PCR as previously described (Canettieri et al.,

2010; Chakrabarti et al., 2002; Gregorieff et al., 2005). *Fos* is a known STAT3 regulated gene (Kinjyo et al., 2006) and its promoter was used as a positive control. PCR primers targeting 25 kb downstream of *Cd44* transcription start site was used as negative control (Cd44neg) along with primers for the *Gapdh* promoter for normalization. The following mouse promoter specific primers were used: STAT3 on *Cd44* promoter (*Cd44* prom); forward: ATGGGCTGGATTTCCACATA, reverse: CCTTTCTCCTCCCAGTCTCC; Negative control primer (25kb downstream of *Cd44* transcription start site) (*Cd44* neg); forward: GACTTCTCCCCCTTTTCTGC, reverse: GCACCTAACCTTCCCTGGTT; STAT3 on *Fos* promoter (*Fos* prom) (positive control) was as described before (Kinjyo et al., 2006); forward: TCTGCCTTTCCCGCCTCCCC, reverse: GGCCGTGGAAACCTGCTGAC; *Gapdh* promoter for normalization; forward: TTGAGCTAGGACTGGATAAGCAGGG, reverse: GTCCGTATTTATAGGAACCCGGATGGTG

Statistical Analysis

Data are presented as mean ± SEM as indicated. Differences in means were analyzed by Student's t-test and one-way ANOVA (for more than 2 groups). Tumor incidence (%) was analyzed by Fisher's exact test. Statistical analyses were performed using GraphPad Prism 7.0 software.

Analyses of Human Samples

Data visualization and statistical analysis were performed using R software version 3.3.2 (R Foundation for Statistical Computing, Vienna, Austria. https://www.R-project.org) and Bioconductor packages. Comparisons of the *CD44* gene expression levels between groups were evaluated using Mann-Whitney U test (2 groups) or Kruskal-Wallis Test (more than two groups). P value < 0.05 was considered as significant (ns: $p > 0.05$, *: $p \leq 0.05$, **: $p \leq 0.01$, ***: $p \leq 0.001$, ****: $p \leq 0.0001$).

Cancer Cell, Volume *33*

Supplemental Information

Liver Cancer Initiation Requires p53 Inhibition by CD44-Enhanced Growth Factor Signaling

Debanjan Dhar, Laura Antonucci, Hayato Nakagawa, Ju Youn Kim, Elisabeth Glitzner, Stefano Caruso, Shabnam Shalapour, Ling Yang, Mark A. Valasek, Sooyeon Lee, Kerstin Minnich, Ekihiro Seki, Jan Tuckermann, Maria Sibilia, Jessica Zucman-Rossi, and Michael Karin

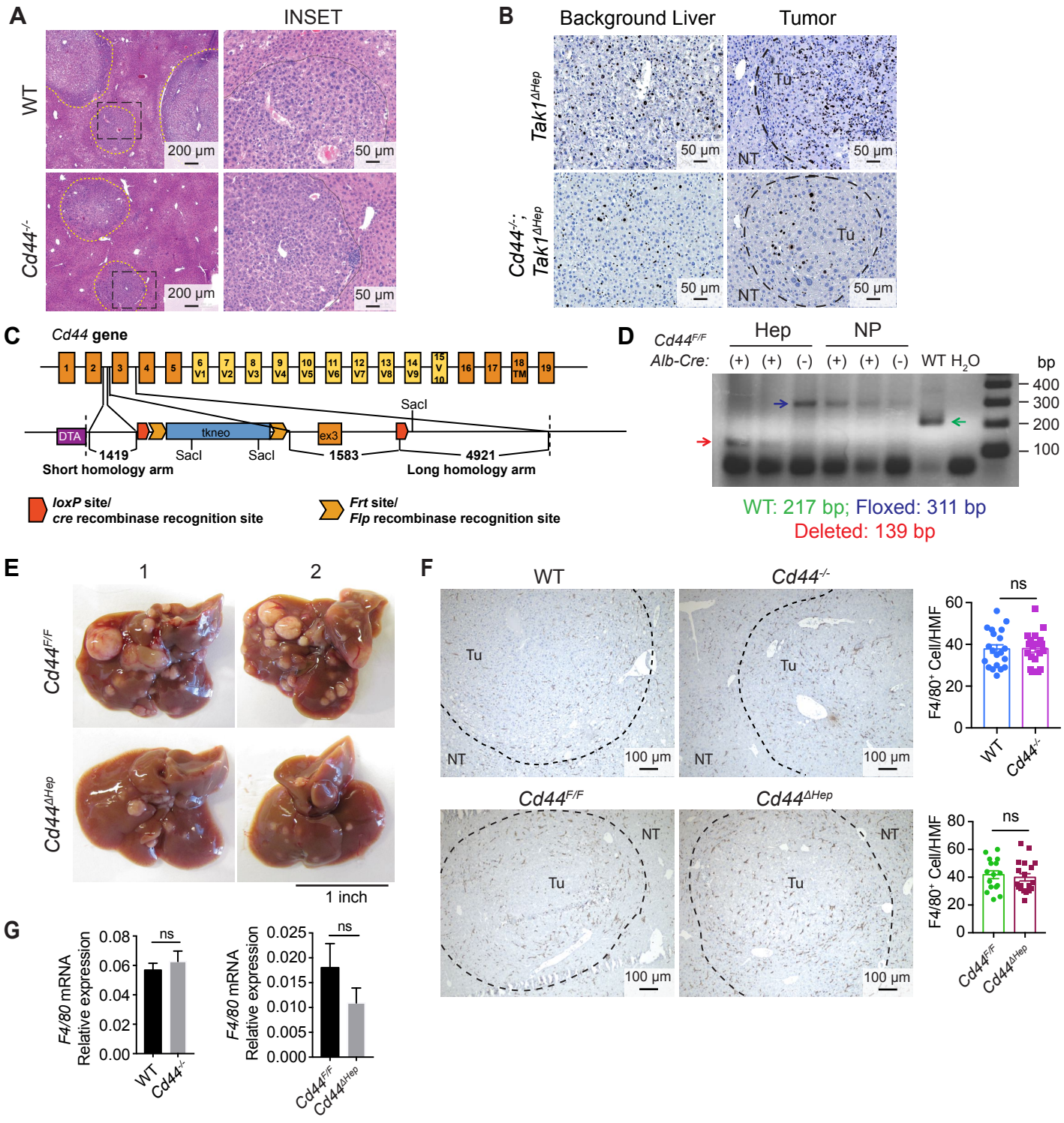

Figure S1. CD44 controls expression of malignancy markers and HCC initiation, Related to Figure 1. (A) Livers from 9-month-old DEN-treated WT and *Cd44*$^{-/-}$ mice were analyzed by H&E staining. Similar size tumors in both genotypes are shown for comparison. (B) Expression of Ki67 was IHC-analyzed in 9-month-old *Tak1*$^{\Delta Hep}$ and *Cd44*$^{-/-}$*;Tak1*$^{\Delta Hep}$ livers. (C) Targeting strategy used for generating *Cd44*$^{F/F}$ mice. The targeting vector contains a 5' DTA cassette for negative selection of the targeted allele, 2 *loxP* sites flanking exon 3, and 2 *Frt* sites used to remove the *TK-neo* cassette after successful positive selection. (D) Genomic DNA extracted from hepatocytes (Hep) and non-parenchymal (NP) cells of the indicated genotypes was PCR-amplified to identify Alb-Cre-mediated recombination and deletion of the floxed allele. (E) Representative images of livers from 9-month-old DEN-treated *Cd44*$^{F/F}$ and *Cd44*$^{\Delta hep}$ mice. (F) Livers of tumor-bearing mice of indicated genotypes were IHC-analyzed for F4/80. Similar size tumors are shown for comparison. Intratumoral F4/80 numbers were quantified per high magnification field (HMF) (n ≥ 19 fields from 5 mice/group). (G) *F4/80* mRNA in tumors from indicated genotypes was quantified by Q-RT-PCR (n ≥ 5 mice/group). All bar graphs represent the mean ± SEM. NT = non-tumor area, Tu = tumor.

Table S1, Related to Figure 1. Summary of the clinical, histological and molecular features of human HCC tumors (INSERM).

Variable		n. of cases	%
Gender (n = 250)	Female	48	19.2%
	Male	202	80.8%
Age (n = 250)	median (min-max)	65 (18-85)	
Histological Diagnosis (n = 250)	HCC	245	98.00%
	HCC on HCA	5	2.00%
Etiology (n = 250)	AL	57	22.80%
	AL HBV	7	2.80%
	AL HBV HCV	1	0.40%
	AL HBV METAB	1	0.40%
	AL HCV	15	6.00%
	AL HM	4	1.60%
	AL METAB	14	5.60%
	HBV	41	16.40%
	HBV HCV	5	2.00%
	HCV	34	13.60%
	HCV METAB	2	0.80%
	HM	17	6.80%
	METAB	16	6.40%
	OTHER	2	0.80%
	W/O Etiology	34	13.60%
Edmonson grade (n = 247)	I	13	5.26%
	II	110	44.53%
	III	100	40.49%
	IV	24	9.72%
Differentiation WHO (n = 249)	Good	72	28.92%
	Medium	135	54.22%
	Weak	42	16.87%
TERT (n = 235)	M	150	63.83%
	NM	85	36.17%
CTNNB1 (n = 237)	M	96	40.51%
	NM	141	59.49%
TP53 (n = 245)	M	53	21.63%
	NM	192	78.37%

Al: Alcohol; HM: Hemochromatosis; M: Mutated; NM: Non-mutated; METAB: Metabolic Syndrome

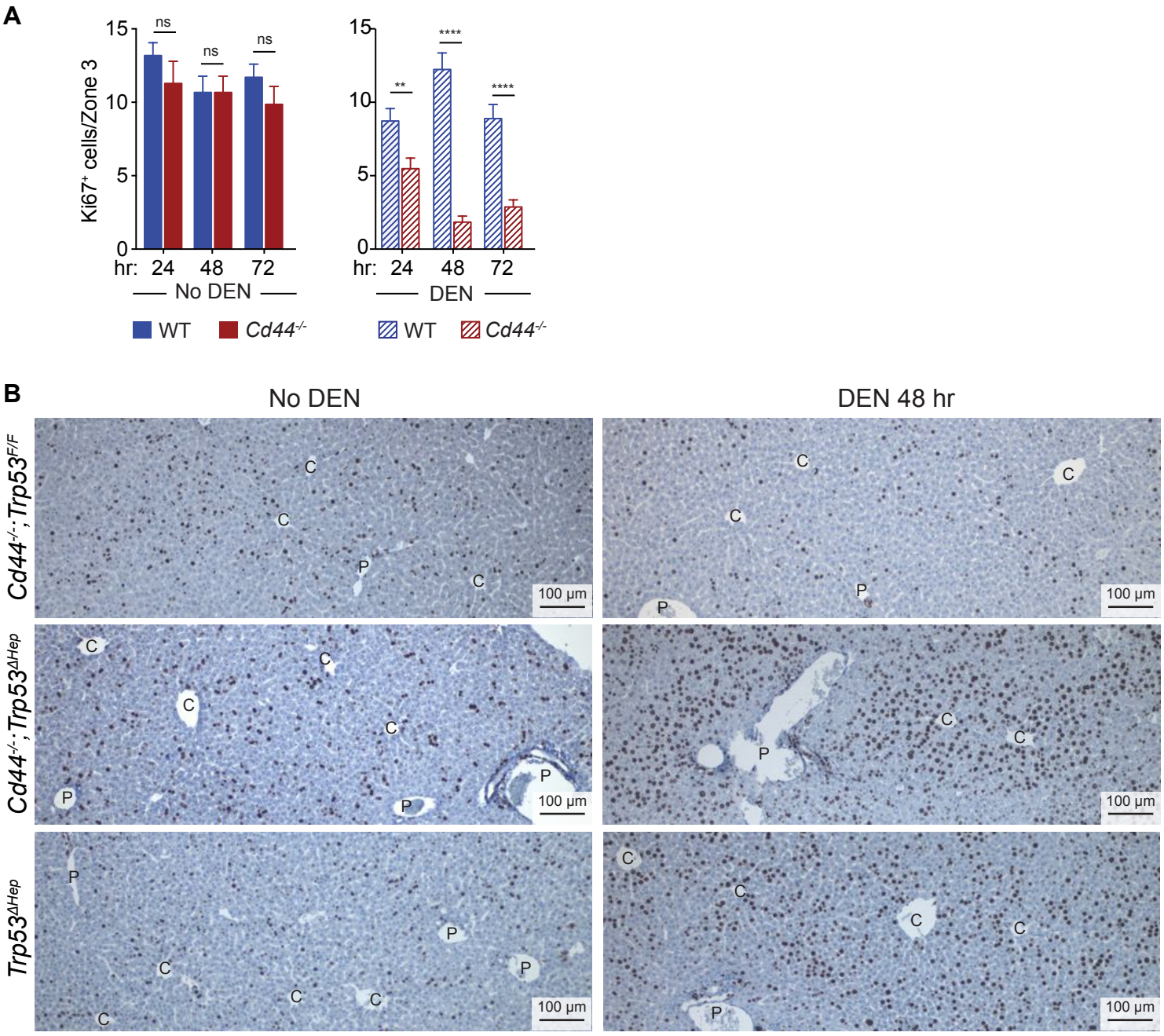

Figure S2. Deletion of *Trp53* rescues cell cycle exit after DNA damage, Related to Figure 2. (A-B) Fifteen-day-old males of indicated genotypes were DEN-challenged (25 mg/kg), their livers were collected when indicated along with age-matched untreated controls, fixed, and stained with Ki67. (A) An alternate representation of the same Ki67 quantitation data shown in Figure 2A (n ≥ 3 mice/group; mean ± SEM). (B) Lower magnification fields of Ki67-stained sections (n ≥ 3 mice/group). (C = pericentral and P = periportal areas).

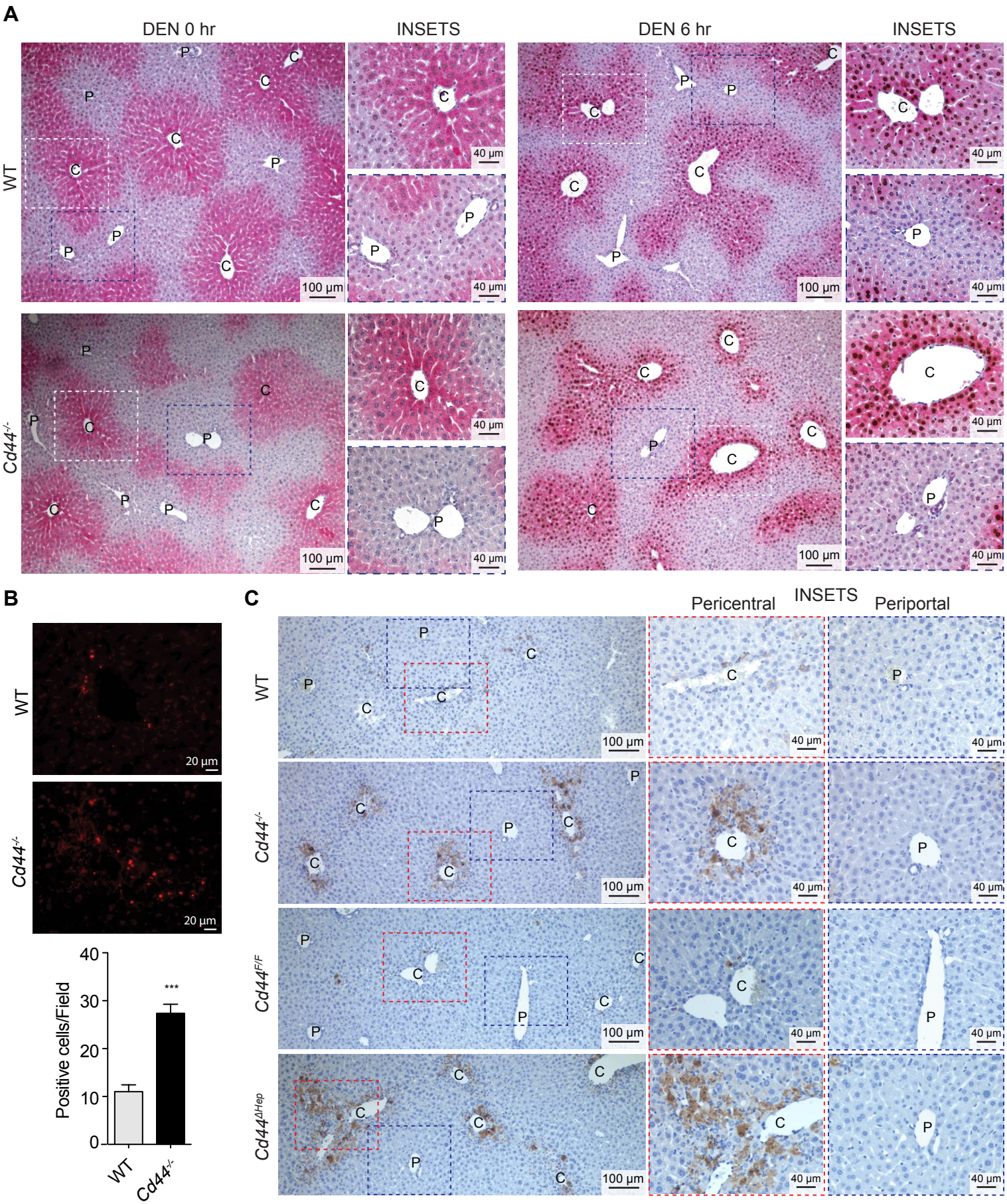

Figure S3. Absence of CD44 predisposes hepatocytes to apoptosis, Related to Figure 3. Male mice of indicated genotypes were DEN-challenged (100 mg/kg), their livers were collected at the indicated time points, and FFPE liver sections were analyzed as indicated. (A) Double IHC staining for Cyp2E1 (indicated by the pink cytosolic stain) and phospho-H2AX (S139) (brown nuclei) (n = 3). (B) TUNEL assay 48 hr post DEN. Bar graphs show numbers of apoptotic cells per 200X field (n ≥ 12 different fields from 3 mice/group; mean ± SEM). (C) IHC staining for CC3 48 hr post DEN (n = 3). C = pericentral and P = periportal areas.

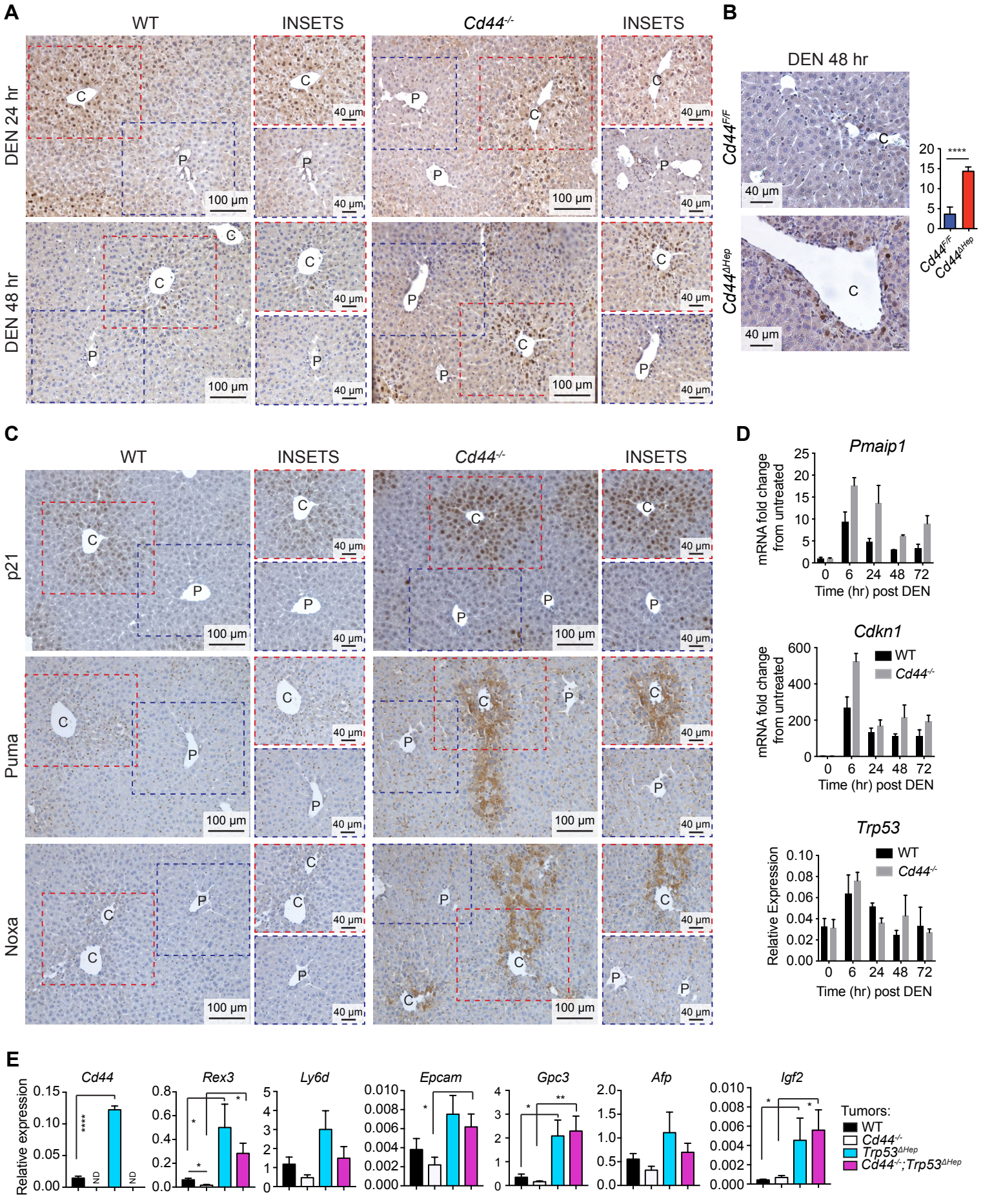
A
WT
INSETS
Cd44-/-
INSETS
DEN 24 hr
DEN 48 hr
C
P
100 μm
40 μm
B
DEN 48 hr
Cd44F/F
Cd44ΔHep
40 μm
****
20
15
10
5
0
Cd44F/F
Cd44ΔHep
C
WT
INSETS
Cd44-/-
INSETS
p21
Puma
Noxa
D
Pmaip1
mRNA fold change from untreated
25
20
15
10
5
0
0 6 24 48 72
Time (hr) post DEN
Cdkn1
mRNA fold change from untreated
600
400
200
0
WT
Cd44-/-
0 6 24 48 72
Time (hr) post DEN
Trp53
Relative Expression
0.10
0.08
0.06
0.04
0.02
0.00
WT
Cd44-/-
0 6 24 48 72
Time (hr) post DEN
E
Cd44
Rex3
Ly6d
Epcam
Gpc3
Afp
Igf2
Relative expression
0.15
0.10
0.05
0.00
****
ND
ND
0.8
0.6
0.4
0.2
0.0
5
4
3
2
1
0
0.010
0.008
0.006
0.004
0.002
0.000
4
3
2
1
0
2.0
1.5
1.0
0.5
0.0
0.010
0.008
0.006
0.004
0.002
0.000
Tumors:
WT
Cd44-/-
Trp53ΔHep
Cd44-/-;Trp53ΔHep

Figure S4. CD44 terminates the p53 response, Related to Figure 4. (A-D) 8-12-week-old male mice of the specified genotypes were DEN-challenged (100 mg/kg), their livers were collected at the indicated times and analyzed as indicated. (A-B) IHC staining for p53 in WT and *Cd44*$^{-/-}$ livers (A); *Cd44*$^{F/F}$ and *Cd44*$^{\Delta Hep}$ livers (B). Quantitation of p53 stained nuclei per HMF is shown to the right of panel B (n = 18, 6 fields per mouse). (C) IHC staining of indicated p53 targets 48 hr post DEN (n ≥ 3 mice/group). (D) Q-RT-PCR analyses of the indicated mRNAs (n = 3). (E) Total RNA isolated from HCC nodules of 9-month-old DEN-treated mice of indicated genotypes was Q-RT-PCR analyzed for expression of the indicated genes (n ≥ 4 tumors/group). All bar graphs represent the mean ± SEM. C = pericentral and P = periportal areas.

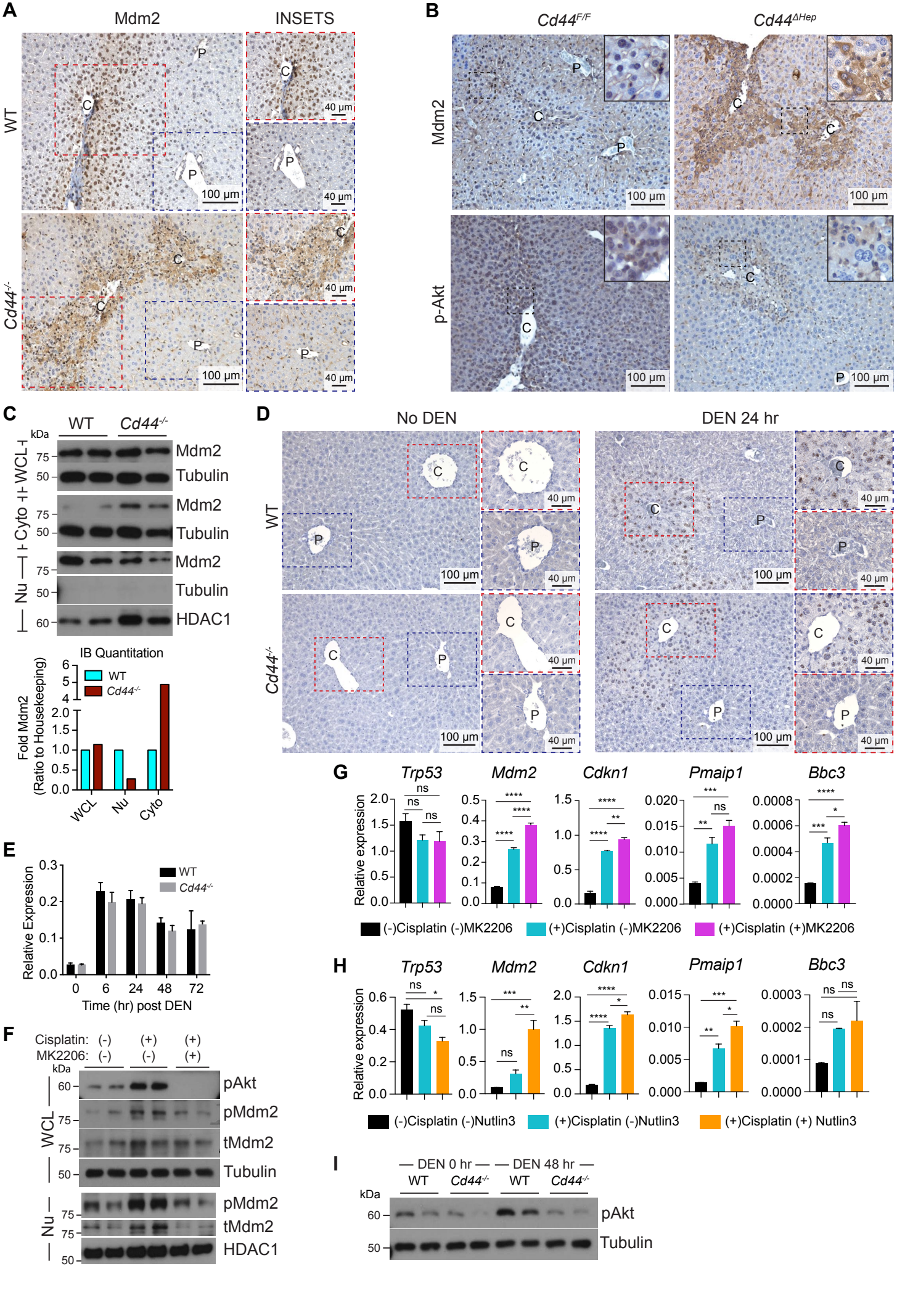
A
Mdm2
INSETS
WT
Cd44-/-
C
P
100 µm
40 µm
B
Cd44F/F
Cd44ΔHep
Mdm2
p-Akt
C
P
100 µm
C
kDa
WCL
Cyto
Nu
Mdm2
Tubulin
HDAC1
75
50
60
IB Quantitation
Fold Mdm2
(Ratio to Housekeeping)
WT
Cd44-/-
WCL
Nu
Cyto
D
No DEN
DEN 24 hr
WT
Cd44-/-
C
P
100 µm
40 µm
E
Relative Expression
WT
Cd44-/-
Time (hr) post DEN
0
6
24
48
72
F
Cisplatin: (-) (+) (+)
MK2206: (-) (-) (+)
kDa
WCL
Nu
pAkt
pMdm2
tMdm2
Tubulin
HDAC1
60
75
50
G
Trp53
Mdm2
Cdkn1
Pmaip1
Bbc3
Relative expression
ns
****
***
**
*
(-)Cisplatin (-)MK2206
(+)Cisplatin (-)MK2206
(+)Cisplatin (+)MK2206
H
Trp53
Mdm2
Cdkn1
Pmaip1
Bbc3
Relative expression
(-)Cisplatin (-)Nutlin3
(+)Cisplatin (-)Nutlin3
(+)Cisplatin (+) Nutlin3
I
DEN 0 hr
DEN 48 hr
WT
Cd44-/-
WT
Cd44-/-
kDa
60
50
pAkt
Tubulin

Figure S5. Mdm2 does not enter the nucleus in CD44-deficient pericentral hepatocytes, Related to Figure 5. (A-E) 8-12-week-old males of the specified genotypes were treated DEN challenged (100 mg/kg), their livers were collected at the indicated time points and analyzed as indicated. (A) IHC staining of FFPE sections for Mdm2 48 hr post DEN. Shown are low and high magnifications of pericentral "C" and periportal "P" regions. (B) IHC for Mdm2 and phospho-S473 Akt 48 hr post DEN. Low and high magnifications of pericentral regions. (C) Livers collected 48 hr post DEN were either homogenized to generate whole cell lysates (WCL) or separated into nuclear (Nu) and cytoplasmic (Cyto) fractions and subjected to IB analyses with the indicated antibodies. The IB bands were quantitated using Image studio software. Mdm2 levels in WCL and Cyto was normalized to Tubulin and Nuclear Mdm2 was normalized to HDAC1 loading control. (D-E) ISH (D) and Q-RT-PCR (E) analysis of *Mdm2* mRNA (n = 3 mice/group for each time point). (F) Dih10 cells were treated with cisplatin (20 μM) in the presence or absence of the Akt inhibitor MK2206 (5 μM). WCL and nuclear fractions were collected 6 hr later and IB-analyzed with the indicated antibodies. (G-H) Dih10 cells were treated with cisplatin (20 μM) in the presence or absence of the Akt inhibitor MK2206 (5 μM) (G) or Nutlin-3 (10 μM) (H). Total RNA was isolated 6 hr post cisplatin treatment and subjected to Q-RT-PCR analyses of p53 target genes. (n ≥ 3 per group). (I) DEN-treated male livers were IB-analyzed with the indicated antibodies. For IB analyses, tissues from two different animals for each genotype/time point, or cell lysates from duplicate treatment wells for each treatment conditions are shown. All bar graphs represent the mean ± SEM.

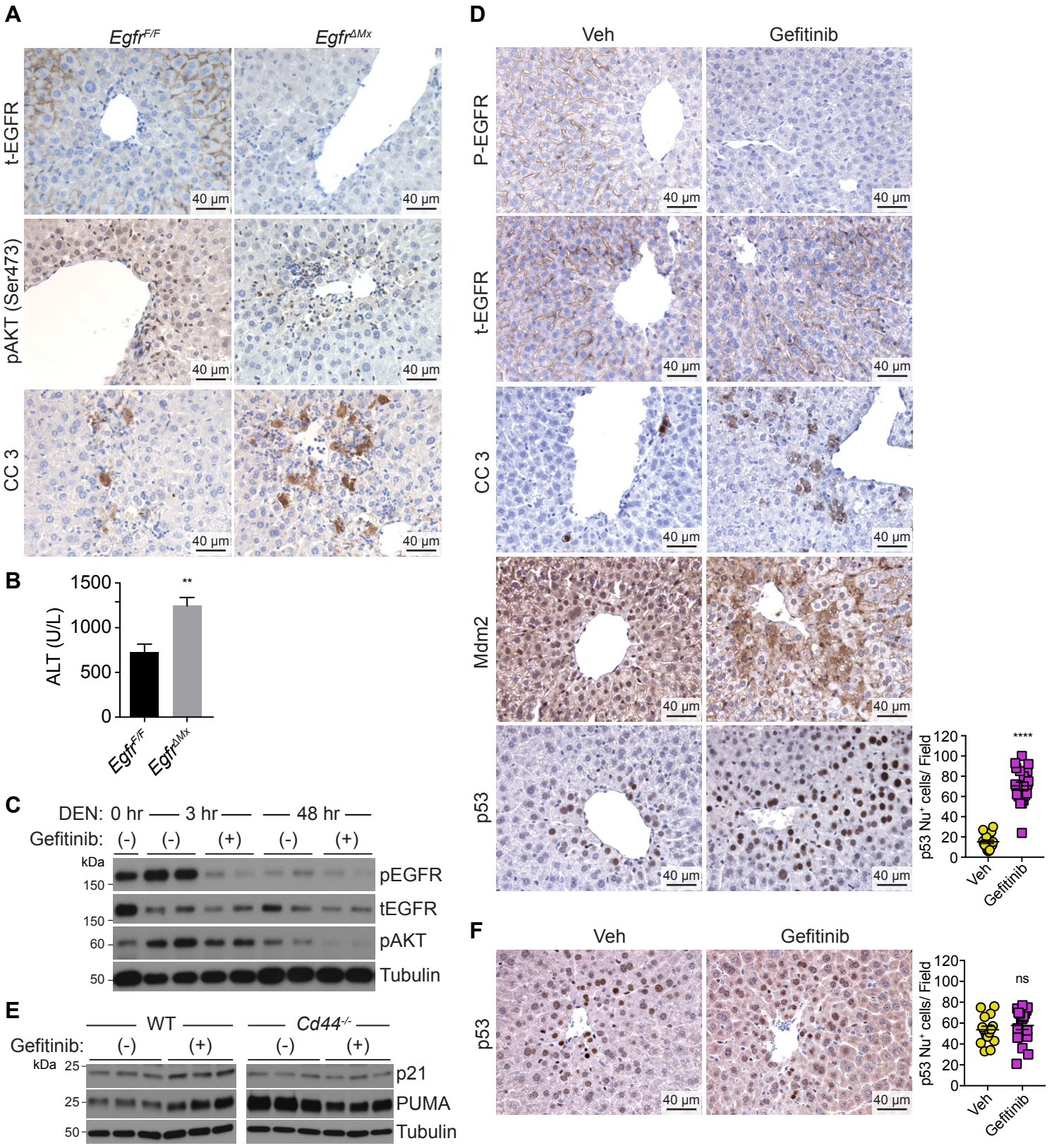

Figure S6. *Egfr* deletion inhibits Akt phosphorylation and induces caspase-3 activation, Related to Figure 6. (A-B) 12-week-old *Egfr*$^{F/F}$ control mice and *Egfr*$^{\Delta Mx}$ mice, in which *Egfr* was deleted using poly (I:C) treatment, were treated with DEN (100 mg/kg). Livers were IHC-analyzed 48 hr post DEN with the indicated antibodies (A) and serum ALT was measured (B). (n ≥ 5 mice/group). (C-D) WT mice were either treated with vehicle or gefitinib (100 mg/kg/day) starting one day prior to DEN injection (100 mg/kg). Livers were collected at 3 and 48 hr after DEN injection and subjected to IB analyses with the indicated antibodies (C) and liver FFPE sections were IHC-analyzed with the indicated antibodies 48 hr post DEN (D). (E-F) Mice of indicated genotypes were treated with either vehicle or gefitinib as mentioned above and livers were IB-analyzed with the indicated antibodies (E), and IHC-analyzed for p53 expression (F) 48 hr post DEN. (n ≥ 15 fields from 3-4 mice/group). All bar graphs and dot plots represent the mean ± SEM.

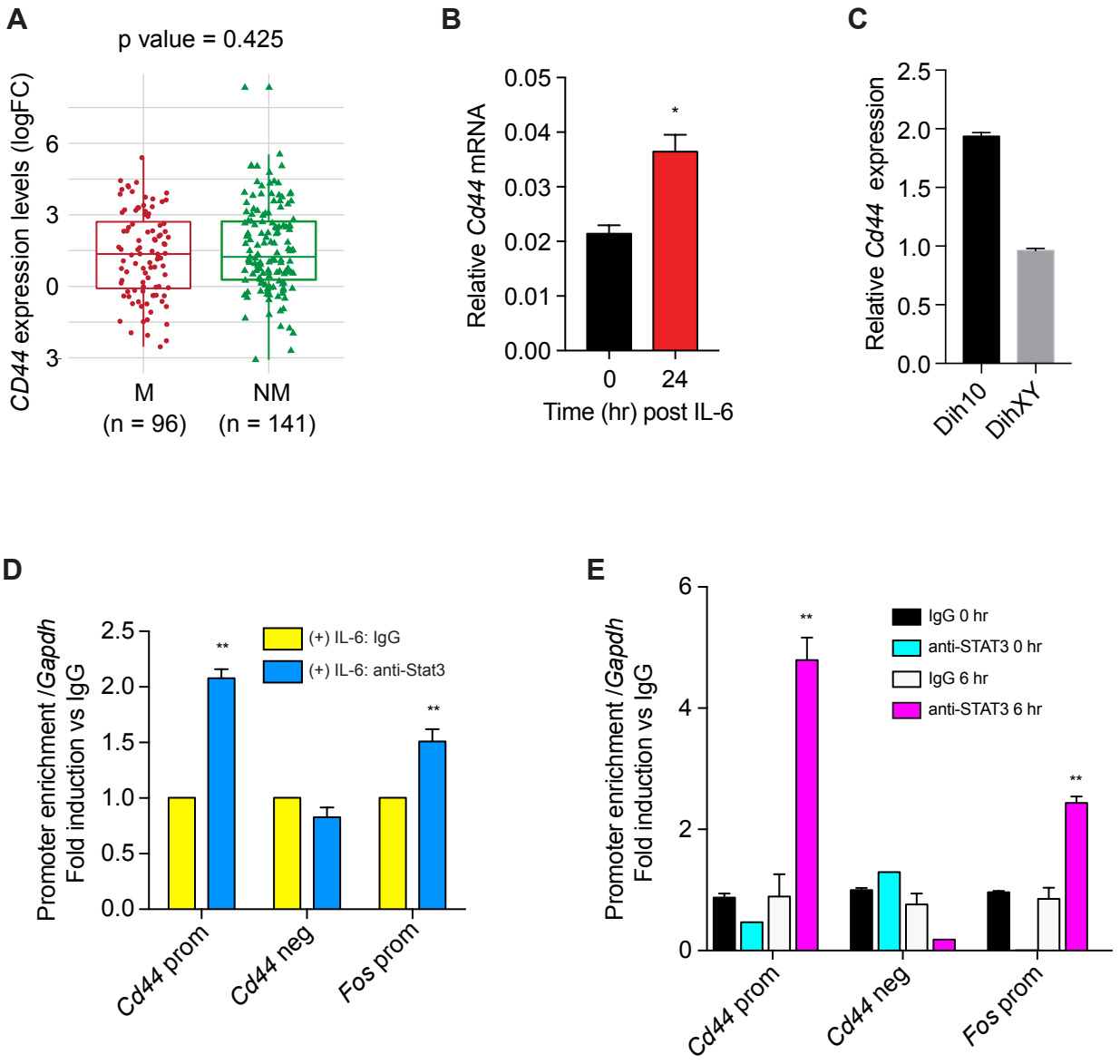

Figure S7. The IL6-STAT3 axis controls *CD44* expression, Related to Figure 7. (A) Human HCC samples (INSERM cohort, Table S1) were categorized into *CTNNB1* activating mutants (M) and non-mutants (NM) and *CD44* expression was analyzed. Results are expressed as Tukey's boxplots where box indicates the 1st and 3rd quartiles, bar indicates median, whiskers indicate 1.5 IQR and data beyond the end of the whiskers represent outliers. (B) Primary hepatocytes from 8-week-old WT mice were stimulated with IL-6 (20 ng/ml). Total RNA was collected at indicated times and *Cd44* mRNA was quantitated by Q-RT-PCR (n=3 per treatment condition). (C) *Cd44* mRNA expression in Dih10 and DihXY cells under normal growth conditions was quantitated by Q-RT-PCR (n=3). (D-E) ChIP assays probing recruitment of STAT3 to the *Cd44* promoter (prom) in IL-6-stimulated (30 min) Dih10 cells (D) and primary hepatocytes collected 0 hr or 6 hr after DEN injection (E) (n=3). All bar graphs in panels B-E represent the mean ± SEM.

Table S2, related to the STAR Methods. Primers used for analyzing changes in gene expression levels.

	Forward	Reverse
mCd44pan	CAAGTTTTGGTGGCACACAG	AGCGGCAGGTTACATTCAAA
mRex3	TACTCCTGGGCCTATCCTTG	GCAGCAGGAGGAGGAAGAG
mIgf2	TGAGAAGCACCAACATCGAC	CTTCTCCTCCGATCCTCCTG
mLy6d	GCCTGGGCACTTCGATGTC	TGAGTTTGCACACTCTTTCCTC
mGpc3	CCCTGAATCTCGGAATTGAA	AGTCCCTGGCAGTAAGAGCA
mAfp	ACAGGAGGCTATGCATCACC	TGGACATCTTCACCATGTGG
mEpcam	CTGGCGTCTAAATGCTTGGC	TCGTACAGCCCATCGTTGTTC
mPmaip1 (Noxa)	GAACGCGCCAGTGAACCCAAC	CTTGGGCTCCTCATCCTGCTG
mBbc3 (Puma)	CTGTGAATCCTGTGCTCTGC	GGTCACACGTGCTCTCTCTA
mS23	CGTCAGGGTGCAGCTCATTA	GGCACGAACGCTGTGATCTT
mCdkn1 (p21)	CGGTGTCAGAGTCTAGGGGA	ATCACCAGGATTGGACATGG
mTrp53	CTAGCATTCAGGCCCTCATC	TCCGACTGTGACTCCTCCAT
mMdm2	CTGCTCTCACTCAGCGATGT	TCTGTGAAGGAGCACAGGAA